Trace and minor elements in galena: A reconnaissance LA-ICP-MS study

Luke George[1], Nigel J. Cook[1], Cristiana L. Ciobanu[1,*], Benjamin P. Wade[2]

[1]Centre for Tectonics, Resources and Exploration (TRaX), School of Earth and Environmental Sciences, University of Adelaide, North Terrace, SA 5005, Australia

[2]Adelaide Microscopy, University of Adelaide, North Terrace, SA 5005, Australia

American Mineralogist (4862 Revision 1)

29th June 2014

ABSTRACT

Minor and trace elements can substitute into the crystal lattice of galena at various concentrations. *In-situ* LA-ICP-MS analysis and trace element mapping of a range of galena specimens from different deposit types are used to obtain minor/trace element data, aimed at obtaining insight into factors that control minor/trace element partitioning. The previously recognized coupled substitution Ag^{+} + $(Bi,Sb)^{3+} \leftrightarrow 2Pb^{2+}$ is confirmed. However, the poorer correlation between Ag and (Bi+Sb) when the latter elements are present at high concentrations (~>2,000 ppm), suggests that site vacancies may come into play: $(2(Bi,Sb)^{3+} + \square \leftrightarrow 3Pb^{2+})$. Galena is the primary host of Tl in all mapped mineral assemblages. Along with Cu, Thallium is likely incorporated into galena via the coupled substitution: $(Ag,Cu,Tl)^{+} + (Bi,Sb)^{3+} \leftrightarrow 2Pb^{2+}$. Tin can reach significant concentrations in galena (>500 ppm). Cadmium and minor Hg can be incorporated into galena; the simple isovalent substitution $(Cd,Hg)^{2+} \leftrightarrow Pb^{2+}$ is inferred. This paper shows for the first time, oscillatory and sector compositional zoning of

* Corresponding author. E-mail: cristiana.ciobanu@adelaide.edu.au

minor/trace elements (Ag, Sb, Bi, Se, Te, Tl) in galena from two epithermal ores. Zoning is attributed to slow crystal growth into open spaces within the vein at relatively low temperatures.

The present data show that galena can host a broader range of elements than previously recognized. For many measured elements, the datasets generated display predictable partitioning patterns between galena and coexisting minerals, which may be dependent on temperature or other factors. Trace element concentrations in galena and their grain-scale distributions may also have potential in the identification of spatial and/or temporal trends within individual metallogenic belts, and as markers of ore formation processes in deposits that have undergone superimposed metamorphism and deformation. Galena trace element geochemistry may also display potential to be used as a trace/minor element vector approach in mineral exploration, notably for recognition of proximal-to-distal trends within a given ore system.

Keywords: Galena, trace elements, Laser-ablation inductively-coupled plasma mass-spectrometry, compositional zoning, substitution mechanisms.

INTRODUCTION

Galena is the most abundant and important lead ore mineral. Despite its simple chemical formula (PbS), a number of additional minor and trace elements can be incorporated into its simple cubic crystal structure. Many of these elements, such as Ag, Bi, Se and Te, can be extracted economically as by-products from an ore containing galena. Others such as Sb, Cd and Tl exist as impurities which may represent an environmental hazard that can be expensive to safely dispose of, or will incur a monetary penalty if present at high enough concentration in a Pb- or Pb-Zn-concentrate. A better understanding the nature and distribution of minor/trace elements in galena is thus invaluable for the minerals industry.

Previous studies of galena (Bethke and Barton 1971; Blackburn and Schwendeman 1977; Tauson et al. 1986; Foord et al. 1988; Foord and Shawe 1989; Liu and Chang 1994; Lueth et al. 2000; Chutas et al. 2008; Renock and Becker 2011) have shown that many minor/trace elements are able to substitute into the crystal lattice at a range of concentrations. Most published work has focused on elements such as Ag, Bi or Sb which are known to occur at relatively high concentrations in some galena specimens (Van Hook 1960; Foord et al. 1988; Foord and Shawe 1989; Jeppsson 1989; Lueth et al. 2000; Costagliola et al. 2003; Chutas et al. 2008; Renock and Becker 2011). Marked gaps in our knowledge exist with respect to the ranges of concentration and inter-element correlations in galena from different types of deposit, and the laws which govern these distributions. Compositional data for galena in a sample suite representative of different styles of ore genesis is also invaluable for constraining the underlying mechanisms of element substitution better than they are at present.

Grain-scale compositional zoning is recognized in many sulfides, e.g., pyrite, arsenopyrite and sphalerite (Hinchey et al. 2003; Chouinard et al. 2005; Di Benedetto et al. 2005; Morey et al. 2008; Cook et al. 2009, 2013a, b; Large et al. 2009), but has not yet been documented as such in galena, and has only been inferred from optical zoning (Ramdohr 1980).

This paper reports a reconnaissance study of elemental trace element analysis of galena from different types of galena-bearing mineral deposits. The aim of this paper was to identify the factors that govern minor/trace element partitioning in galena, and also determine elemental trends and correlations and consider whether specific minor/trace elements are released or retained in the galena structure during syn-metamorphic recrystallization at different facies conditions.

Although many of our findings are preliminary and may deserve verification by additional studies, we believe that, alongside geometallurical applications, the grain-scale distribution of trace elements in galena has application in ore genesis, and potentially also in mineral exploration.

The approach here is analogous to that of sphalerite and bornite/chalcocite described in Cook et al. (2009b, 2011), respectively. The sample suite used in this study is representative of a range of Pb-Zn

ores from different deposit types and from different metallogenic provinces worldwide (Table 1, Fig. 1). The mineralogy and petrography of each sample is characterized using optical and scanning electron microscopy (SEM), and *in-situ* laser-ablation inductively-coupled plasma mass spectrometry (LA-ICP-MS) to obtain trace element data with detection limits well below 1 ppm for many heavier elements. LA-ICP-MS trace element mapping is used to detect minor/trace element heterogeneity at the scale of single grains.

Integral to any research into minor/trace element distributions in a mineral is the ability to distinguish between the presence of any given element in solid solution from the same element occurring as micro-scale inclusions of a distinct mineral phase. Although not able to directly prove the existence of solid solution or micro-inclusions, LA-ICP-MS can provide support for the mode of occurrence of a given element. If sufficiently large and/or heterogeneously distributed, micro-inclusions will be noticeable on the time-resolved ablation down-hole profiles.

BACKGROUND

In recent times, multi-element microanalytical techniques with ppm-level precision and μm-scale spatial resolution have become readily available (e.g., LA-ICP-MS and Electron Probe Microanalysis (EPMA)), resulting in the generation of large amounts compiling the abundance of minor/trace elements in the common sulfides (e.g., Cook et al. 2009a, b, 2011; Large et al. 2009; Ye et al. 2011; Winderbaum et al. 2012; Ciobanu et al. 2013; Reich et al. 2013). Development of high-resolution scanning electron microscopy and chemical mapping techniques at the 0.1-1 μm-scale has shown extraordinary compositional heterogeneity in many sulfides, even those previously considered not to display compositional inhomogeneity such as molybdenite (Ciobanu et al. 2013). One implication of these studies is that much of the published minor/trace element data, especially those obtained before the modern era, may simply represent averages of more than one compositionally-distinct zone within a

given mineral. The published data for galena summarized below nevertheless provides a foundation for understanding the range and quantities of minor/trace elements that can be incorporated.

Silver, bismuth, antimony and arsenic

Substitution of silver into galena represents a well-characterized example of solid solution. Monovalent Ag is virtually insoluble via the simple $2Ag^{+} \leftrightarrow Pb^{2+}$ substitution (maximum 0.4 mol.% at 615 ^{o}C; Van Hook 1960) due to the requirement that one of the two silver atoms must be placed in a structurally unfavorable interstitial position in the galena lattice. Pring and Williams (1994) concluded that in the absence of Bi or Sb, substitution of Ag into PbS in solid solution will not exceed 0.1 mol.%, and that Ag formed inclusions of native silver that showed no crystallographic relationship with host galena. In past studies, high concentrations of Ag in galena have been commonly explained by the presence of sub-micron scale of inclusions of acanthite (Ag_2S (e.g., Krismer et al. 2011)), and if both Sb and Bi are present, explained by the exsolution of phases such as miargyrite or matildite. Attempts to identify the chemical state of Ag in galena by XANES methods (Giuli et al. 2005) also identified that inclusion-hosted Ag dominated over that of solid solution.

If aided by the presence of Bi^{3+} and/or Sb^{3+} (and potentially other trivalent cations), significant quantities of Ag can be added to the galena structure via the coupled substitution $Ag^{+} + (Bi,Sb)^{3+} \leftrightarrow 2Pb^{2+}$ (Chutas et al. 2008; Renock and Becker 2011). This substitution results in the octahedral sites left by two Pb^{2+} ions being fully occupied by Ag^{+} and $(Bi,Sb)^{3+}$ (Costagliola et al. 2003). In nature, galena commonly displays wide variations in Ag, Bi and Sb concentrations (Lueth et al. 2000). Below 420 ^{o}C, there is incomplete but substantial solid solution between galena and the two end-members matildite ($AgBiS_2$) and miargyrite ($AgSbS_2$), and complete solid solution above this temperature (Van Hook 1960; Wernick 1960; Hoda and Chang 1975; Amcoff 1976; Sharp and Buseck 1993; Ghosal and Sack 1999). Silver solubility in galena has been shown to reach 9.4 wt.% between 350 and 400 ^{o}C via this coupled substitution mechanism (Foord et al. 1988; Foord and Shawe 1989). Chutas et al. (2008)

demonstrated that Bi is preferred to Sb in the coupled substitution. Although rare, in an analogous coupled substitution together with Ag^+, As^{3+} can also be substituted into galena.

Coupled substitution indicates that the maximum possible mol.% Ag within the galena lattice should not exceed mol.% (Bi+Sb). If mol.% Ag > mol.% (Bi+Sb), the presence of sub-micron-scale inclusions of Ag-minerals can be inferred. Common Ag-bearing phases observed as inclusions in galena include acanthite, Ag-Cu-Sb- or Ag-Cu-As-sulfosalts, and Ag-tellurides and sulfotellurides (Sharp and Buseck 1993; Lueth et al. 2000; Cook and Ciobanu 2003).

Costagliola et al. (2003) showed that metallic silver (Ag^0) is an insignificant component in natural galena. As with other sulfides, electrum inclusions will be more widespread if Au is also present (Knipe et al. 1992; Larocque et al. 1995). Scaini et al. (1997) have however demonstrated that Ag^0 can be taken into galena through sorption of Ag^+ onto the surface of a galena, and the subsequent oxidation/sulfidation of Ag^+ through ion exchange. This process may only occur naturally in environments poor in Bi or Sb, when Ag cannot be preferentially incorporated into the galena lattice via coupled substitution(s) (Jeppsson 1989).

In the case that mol.% (Bi + Sb) exceeds mol.% Ag in galena, micro-inclusions of Bi- or Ag-bearing phases (miargyrite, matildite etc.) can be inferred. When Sb is dominant, common inclusion minerals include myargyrite, stibnite (Sb_2S_3), tellurantimony (Sb_2Te_3), or Ag-(Cu)-Pb-Sb-sulfosalts. When Bi is dominant, common inclusion minerals will include bismuthinite (Bi_2S_3) and matildite; if Te is also present, minerals of the tetradymite group (Bi_xTe_y; Cook et al. 2007) may dominate. In other samples where mol.% (Bi + Sb) exceeds mol.% Ag, there is a possibility that Bi and/or Sb substitute into galena without Ag, necessitating site vacancies to maintain charge balance.

Thallium and copper

Thallium is commonly found in galena at concentrations up to 20 ppm (Nriagu 1998). Graham et al. (2009) report "measurable concentrations of Tl in galena from the Drenchwater sediment-hosted

massive sulfide deposit, Brooks Range, Alaska, but note that these are an order of magnitude less than in pyrite from the same deposit. Despite the fact that the intermediate phase $TlPbSbS_3$ has been identified (Balić-Zunić and Bente 1995), there is no evidence to suggest solid solution between $TlSbS_2$ and PbS, implying the coupled substitution $Tl^{+} + Sb^{3+} \leftrightarrow 2Pb^{2+}$.

Blackburn and Schwendeman (1977) report up to 70 ppm Cu in galena. They attributed the copper to the monovalent state, and believed it was involved in similar coupled substitutions as Ag.

Selenium and tellurium

Clausthalite (PbSe) forms a continuous solid solution with galena above 300 °C, allowing for several wt.% Se to be present in galena (Liu and Chang 1994). Intermediate compositions along the PbS–PbSe join are widely reported (e.g., Coleman 1959), however a continuous solid solution between galena and altaite (PbTe) does not exist. This is due to miscibility gaps between end-members below 805 ^{o}C (Darrow 1966; Liu and Chang 1994), commonly resulting in micron to sub-micron scale inclusions of altaite within galena.

Cadmium, mercury and manganese

Bethke and Barton (1971) and Tauson et al. (1986) demonstrated that Cd and Hg could be incorporated into galena via solid solution. Foord et al. (1988) reported concentrations of Hg in natural galena from the Round Mountain and Manhattan Gold Districts, Nevada. Unpublished data from Bethke and Barton (1971) claimed that galena could incorporate as much as 25 mol.% CdS in solid solution at the eutectic temperature of 950 ^{o}C. From incomplete experiments they also concluded that Mn can be incorporated into galena up to a maximum of 3.5 mol.% MnS. Tauson et al. (1986) report much lower solubility of CdS and HgS in galena (1.5 and 1 mol.%, respectively), and considered partitioning of Hg between coexisting galena-sphalerite pairs as a potential geothermometer. However in a later paper, Tauson et al. (2005) showed that Cd and Hg could be adsorbed onto the surface of

galena crystals, leading to the conclusion that the concentrations of Cd and Hg in galena reported earlier were 1-2 orders of magnitude too high, and that the solubility limits of structurally-bound Cd and Hg may be much lower.

SAMPLES AND METHODOLOGY

Background geology of ore samples

Forty-one samples of Pb-Zn ores were analyzed from 15 representative deposits worldwide (Fig. 1, Table 1; see references therein). The two best represented deposit types are metamorphosed sedimentary-exhalative (SEDEX) deposits (7) and epithermal deposits (5). Three other deposit types are also included: skarn (Băița Bihor, Romania); non-metamorphosed ophiolite-hosted massive sulfides (VHMS) (Vorța, Romania); and an orogenic gold deposit (Lega Dembi, Ethiopia).

The epithermal group includes examples from orogenic belts in Central Asia (Kochbulak, Uzbekistan), and SE Europe (Romania and Bulgaria), with ages ranging in age from Paleozoic to Neogene. Due to their affiliation with relatively young magmatic-hydrothermal systems in volcano-plutonic arcs, all these deposits are known for their varied mineralogy and include Pb-Ag-Sb-As or -Bi sulfosalts.. Galena sampled include those from base metal veins that are satellite to high-grade Au orepipes (Kochbulak), or porphyry Cu-Au stocks (Elatsite, Bulgaria). Galena was also sampled from a magmatic-hydrothermal breccia with Pb-Zn and Au orefield zonation (Baia de Arieş, Romania), and from typical polymetallic veins (Pb-Zn-Ag veins from Herja, Baia Mare District, Romania, and Cu-Au-Pb-Zn veins from Toroiaga, 90 km to the east; both systems relating to the same regional-scale E-W-trending Dragos Voda fault (Neubauer et al. 2005 and references therein)). The Toroiaga veins are considered to have formed at temperatures of as much as 400 °C (Cook 1997), unlike most deposits in the Baia Mare district *sensu stricto* which are typical Pb-Zn+Ag veins. The Vorța and Baia de Arieş deposits define the start and end of a succession of Alpine magmatic-hydrothermal events in South

Apuseni Mts. spanning from the Jurassic (ophiolite-hosted seafloor syngenetic volcanogenic massive sulfides) to Neogene (Golden Quadrilateral (GQ); Ghițulescu and Socolescu 1941; Vlad and Borcos 1997; Ciobanu et al. 2004). Both deposits are known for their controversy regarding overlapping between younger and older styles of mineralization.

Băița Bihor and Elatsite are located hundreds of km apart but belong to the same Late Cretaceous Banatitic Magmatic and Metallogenetic Belt (BMMB), which is recognized for a widespread Bi-signature throughout all mineralization styles (e.g., Ciobanu et al. 2002). The largest number of samples in this study (8) are represented by those from Băița Bihor, , and has the most diverse sulfide mineralogy (As-, Sb- and Bi-sulfosalts as well as Bi- and Ag-tellurides; Cioflica et al. 1995, 1997; Ilinca and Makovicky 1999; Cook and Ciobanu 2003; Ciobanu et al. 2011, 2014; Ilinca et al. 2012), and most complex geochemical signature (Bi-Ag-W-Se-Te-Ni-Co-Sn) among the 15 deposits. Here, the Pb-Zn ores are characteristic of distal ore at the marble/skarn contact in each Cu-dominant orepipe (Antoniu and Antoniu North), and form distinct Pb-Zn orebodies such as Marta several hundred meters away. Minor galena+sphalerite also occurs within the inner part of Cu-orebodies.

The SEDEX group (Table 1; see references therein) includes giant/large Proterozoic deposits from several cratonic/shield areas such as Broken Hill (NSW, Australia), Mt. Isa (Qld., Australia), Sullivan (BC, Canada), or smaller deposits such as Zinkgruvan (Bergslagen, Sweden). Ore deposits within this group have undergone variable metamorphism ranging from granulite facies (Broken Hill) to greenschist facies (Mt. Isa). Included in the same group are two smaller deposits (Bleikvassli and Mofjellet) from the (Lower Paleozoic) Norwegian Caledonides, and an occurrence (Kapp Mineral) from the Svalbard Archipelago of undetermined age (mineralization occurs along Tertiary faults at the contact between Late Proterozoic and Paleozoic sequences). Each of the 7 SEDEX deposits has undergone regional metamorphism (Table 1), however unequivocal textural evidence for recrystallization of the sulfide assemblages is only seen in those metamorphosed above greenschist facies. Textural evidence of recrystallization is absent in samples from Mt. Isa, Sullivan and Kapp

Mineral, but evident in samples from Mofjellet, Bleikvassli and Broken Hill which display coarse annealed textures, commonly with 120° triple junctions between grains. Recrystallization at peak metamorphic conditions should allow equilibrium partitioning of elements between coexisting minerals. In that respect, peak metamorphism conditions (Table 1) will only give upper temperature limits for co-crystallization of sulfide assemblages. Similar to the epithermal deposits, these deposits (except Kapp Mineral) display a diverse mineralogy as a response to remobilization during the metamorphic overprint (e.g., Cook et al. 1998).

The Lega Dembi deposit, Ethiopia, is of orogenic Au type. It is included here due to its unusually Pb-rich character, and since galena and different Pb-As- and Pb-Sb-sulfosalts, tellurides and selenides are associated with Au deposition (Cook et al. 2001). Inclusion of this deposit thus enables comparison of trace element geochemistry of galena in sulfide assemblages crystallized at comparable temperatures during formation as regional metamorphic overprinting, but in different styles of mineralizing system (i.e., orogenic Au vs. metamorphosed SEDEX), as well as between telluride-rich Au deposits of different types (i.e., epithermal and orogenic Au; Cook et al. 2009c).Prepared as a one-inch polished block, each sample was examined by optical and scanning electron microscopes. Figure 2 displays various occurrences of galena, and its associated textures. Cleavage patterns in coarse galena highlight the difference between crystallization in open spaces (skarn), and under superimposed deformation during metamorphism (Fig. 2a, b). Comparison of sulfide assemblages from metamorphosed SEDEX deposits show that those that underwent metamorphism at amphibolite facies are coarser-grained and display mutual boundaries, interpreted to represent equilibrium during re-crystallization. In contrast, deposits metamorphosed at greenschist facies retain primary (inherited) textures relating to syn-sedimentary precipitation, such as fine intergrowths between sulfides (Fig. 2c-f).

Experimental

Back-scattered electron (BSE) imaging allowed characterization of mineral inclusions within galena, and was used in selecting areas for trace element analysis and element mapping.

Quantitative trace element compositional data for galena ('spot analyses') was obtained using a New Wave UP-213 Nd:YAG laser-ablation system coupled to an Agilent HP-7500 inductively coupled plasma mass spectrometer (Adelaide Microscopy, University of Adelaide). Beam diameter was set at a constant 30 μm, with a repetition rate of 4 Hz and energy set to produce a fluence at the sample of ~0.5 Jcm^{-2}. Data were collected using time-resolved data acquisition in fast peak-jumping mode, and calculations were carried out using GLITTER data reduction software (Van Achterberg et al. 2001). Total acquisition time for each analysis was 80 s, with 30 s background measurement followed by 50 s of sample ablation. Further details can be found in other recently published accounts of LA-ICP-MS analysis of sulfides in our laboratory (Cook et al. 2013b; Ingham et al. 2014).

Every precaution was taken to ensure analyzed areas were free of inclusions large enough to be seen by SEM back-scatter electron imaging. Despite this, when using a spot diameter large enough to achieve sub-ppm precision, the LA-ICP-MS technique cannot always resolve chemically-distinct, exsolved phases at sub-surface, particularly when they are only present at the submicron level. Based on SEM inspection of ablation craters, the approximate ablation rate for galena is ~0.6-1.0 μm/sec.. Thus if they do exist, during ablation one could potentially drill through submicron layers of phases very quickly. The smooth time-resolved depth spectra can therefore represent an averaging effect due to the limited depth resolution, which is in turn a result of the rapid ablation rate of galena, and the large list of elements giving a long sweep time. Similarly, the lateral resolution is limited by the size of the laser spot. If the analyzed area is finely zoned across the grain, then a spot may well stretch across multiple zones, giving an average concentration.

Calibration was performed against the MASS-1 sulfide reference material formerly known as PSD-1 (Wilson et al. 2002) The BCR-2G silicate glass reference material (Wilson 1997) was used as a

secondary check (running it as an 'unknown') given that the MASS-1 reference material, although matrix-matched, is not well suited for analysis if used alone.

MASS-1 contains a small amount of Pb compared to galena. The response of the electron multiplier is linear over 9 orders of magnitude, and an electron multiplier Pulse to Analogue calibration is carried out at the beginning of every run, and as a result in our view the cps/ppm yield is not considered a significant issue when using standards with a low amount of the internal standard compared to the unknown (c.f. the analogous case for molybdenite; Ciobanu et al. 2012). However, the major element composition of the MASS-1 is substantially different to galena, which could infer there are matrix effects that are not quantifiable at present. Danyushevsky et al. (2011) investigated the suitability of an analogous sulfide standard (STDGL2b2, containing 1,216 ppm Pb) for the analysis of galena. Using Pb as an internal standard, Danyushevsky et al. (2011) analyzed pressed-powder pellets by XRF and solution ICP-MS. Results showed that standard analytical errors resulting from matrix-dependent fractionation were low (<15%) but can be as high as 50% for W, Zn and Cd. Validation of MASS-1 for the analysis of galena is beyond the scope of the present paper. Even if the absolute numbers reported in this reconnaissance study are not 100% accurate, they are nevertheless systematic given the constant major element composition of galena. Thus any differences in trace element concentrations are considered to be internally consistent.

Batches of twelve analyses were bracketed by repeat analyses of the external standards, allowing monitoring of, and correction for, instrumental drift. A linear drift correction based on the analysis sequence and on the bracketing analyses of MASS-1 was applied to the count rate for each sample. Assuming 100% PbS composition, lead calculated from measurement of ^{208}Pb was used as the internal standard for galena analysis.. The following suite of isotopes were analyzed: ^{33}S, ^{34}S, ^{53}Cr, ^{55}Mn, ^{57}Fe, ^{58}Fe, ^{59}Co, ^{60}Ni, ^{65}Cu, ^{66}Zn, ^{69}Ga, ^{75}As, ^{82}Se, ^{95}Mo, ^{107}Ag, ^{111}Cd, ^{115}In, ^{118}Sn, ^{121}Sb, ^{125}Te, ^{182}W, ^{197}Au, ^{202}Hg, ^{205}Tl, ^{204}Pb, ^{206}Pb, ^{208}Pb and ^{209}Bi. The two sulfur- and iron-isotopes were monitored to check for internal consistency. Mean minimum detection limits (mdl) for each element in each sample are

given in Electronic Appendix A. Errors are reported in GLITTER as 1σ based on counting statistics for signal and background. The equations are propagated throughout the calculations assuming a 1% relative uncertainty on the elemental concentrations in the reference material, and a 3% relative uncertainty on the values of the internal standard. Precision values for each element in each sample are given in Electronic Appendix A – typically 10-30% for most elements present at measurable concentrations throughout the sample suite but higher for elements such as In, Hg and Au which never exceed a few ppm. It proved difficult to obtain low mdl values or good precision values for Se due to poor signal to background ratios. These problems resulted in variable mdl's, including both a small number of extremely high mdl values, as well as other extremely low values (<0.00001) that cannot be regarded as reliable.

The spot analytical uncertainty output in GLITTER is a combination of internal (counting statistic noise of the measurements over the length of analysis) and external signal uncertainties (mass bias, correction of unknowns to standards, laser induced elemental fractionation (LIEF), instrument drift). Assuming a stabilised cell, the largest contribution to analytical uncertainty will be LIEF, followed by counting statistics, followed by instrument drift. To minimize LIEF, the spot size, frequency, and fluence are identical from standards to unknowns. Additionally, dwell times are kept as long as reasonably possible (0.05 s. for all elements except Ag, Sb and Bi (0.03 s.) and S and Pb (0.007 s.), and the method is run for as long as reasonably possible, to get better counting statistics. Standards are run as often as reasonably possible to minimize any errors in the linear fit drift correction.

Four LA-ICP-MS element maps were made on selected areas ranging in size from approximately 1 to 4 mm^2. In order to obtain a visual image of minor/trace element distribution within grains, mapping focused on areas of the galena grains in which compositional zoning was suspected.. LA-ICP-MS mapping was carried out using a Resonetics M-50-LR 193-nm Excimer laser coupled to an Agilent 7700cx Quadrupole ICP mass spectrometer (Adelaide Microscopy). The M-50 instrument utilizes a two-volume small volume ablation cell (Laurin Technic Pty. designed for excellent trace element

sensitivity) (Müller et al. 2009). Ablation was performed in an atmosphere of UHP He (0.7 l/min), and upon exiting the ablation cell the aerosol is mixed with Ar (0.93 l/min), after which the mix is passed through a pulse-homogenizing device or "squid" prior to direct introduction into the torch. The ICP-MS was optimized daily to maximize sensitivity on isotopes of the mass range of interest, while keeping production of molecular oxide species (i.e., $^{232}Th^{16}O/^{232}Th$) and doubly charged ion species (i.e., $^{140}Ce^{2+}/^{140}Ce^{+}$) as low as possible, and usually <0.2%.

Imaging was performed by ablating sets of parallel line rasters in a grid across the sample. A consistent laser beam size (9 μm) and 10 μm/s scan speed were chosen to give the desired sensitivity of elements of interest, and adequate spatial resolution for the study. The spacing between the lines was kept at a constant 9 μm to match the size of the laser spot. A laser repetition of 10 Hz was selected at a constant energy output of 80 mJ, resulting in an energy density of ~4 Jcm^{-2} at the target. A set of 29 elements were analyzed with dwell times of 0.01 s. for all elements, apart from In, Au and Tl (0.05 s.), resulting in a total sweep time of 0.436 s. A 30 second background acquisition was acquired at the start of every raster, and a delay of 20 s followed each line to allow for cell wash-out, gas stabilization, and computer processing time. Identical rasters were done on the MASS-1 reference material at the start and end of a mapping run.

Element maps were compiled and processed using the program Iolite developed by the Melbourne Isotope Group (Paton et al. 2011). Iolite is an open source software package for processing ICP-MS data, and is an add-in for the data analysis program Igor developed by WaveMetrics. A typical mapping run was analyzed over a 6-20 hour-session, in which significant instrument drift could occur. To correct for this, standards were analyzed immediately before and after the run to assess drift. If present, a correction was applied using a linear fit between the two sets of standards. Following this, the average background intensity of every element was subtracted from its corresponding raster, the resultant time resolved intensities compiled into a 2-D image displaying combined background/drift corrected intensity for each element. To produce the quantitative 2-D concentration maps from these intensity

rasters, a sulfur value of 25 wt.% was used as the internal standard. This value is intended to represent an average sulfur wt.% value for an assemblage comprising galena, sphalerite and chalcopyrite. We have tested the accuracy of the ppm values on the four maps in this contribution by subsequent spot analysis on the same grains, and found agreement to be excellent.

RESULTS

LA-ICP-MS trace element data

The LA-ICP-MS minor/trace element data for galena (mean element concentrations, standard deviations, and minimum and maximum concentrations) is summarized in Table 2. The table includes data for 12 elements present at measurable concentrations in one or more sample group. Although we endeavored to analyze only those volumes free of inclusions, some analyses did show anomalous concentrations of Cu or other elements, which were likely the result of mineral inclusions beneath the sample surface. Representative LA-ICP-MS depth profiles are shown in Figure 3, demonstrating both smooth profiles indicative of elements in solid solution, and irregular profiles suggesting the presence of inclusions. The spot analyses inferred to contain inclusions were not included in calculations of statistics.

The mean concentrations of key elements in individual samples are plotted as cumulative plots in Fig. 4. These allow a visualization of both the range of absolute values for each element, and the variance within each sample and deposit type. The larger standard deviations relative to means for the epithermal group reflect the intra-crystal compositional zoning descried below. Bismuth, Sb, Ag and Se have consistent and relatively high concentrations in galena throughout the 5 deposit types (Fig. 4). Despite being in high concentration, Bi, Sb, Ag, and Se display a spread of at least two orders of magnitude within each group of deposits, or individual deposits such as Băița Bihor. Other elements (Tl, Sn, Cd, Te etc.) display comparable concentration ranges between deposit types, except for the

SEDEX group in which Bleikvassli has the highest values among all deposits for Tl and Sn, and Mofjellet is highest for Te within this group. There is a clear difference between the relative concentrations of Bi, Te and Sb in the skarn group compared to the epithermal and SEDEX groups. The latter are clearly enriched in Sb relative to Bi and Te. In contrast, Ag and Se show comparable ranges of variation for all three groups. In skarn galena analyses, the proximal-to-distal trend is expressed by relative enrichment of Bi, Ag and Te in proximal galena, and Sb-enrichment in distal galena. Individual deposits within the SEDEX category appear to contain similar concentration ranges of several elements (e.g., Bi, Tl, Sn and Te). In contrast, the epithermal group displays greater variation, possibly reflecting the broader variety of environments. Galena from VHMS ores at Vorța is compositionally closer to the epithermal rather than skarn trend within the Apuseni Mts. deposits.

Silver

Silver has some of the highest measured concentrations in galena with respect to any other element analyzed, with means within a single sample ranging from 95.5 ppm in BH218 (Broken Hill) to 14,928 ppm in BB55 (Băița Bihor). Smooth time-resolved LA-ICP-MS down-hole profiles and low standard deviations for the Ag concentration in each sample (averaging just 21%), strongly support that the measured Ag is in solid solution and is not the result of sub-µm inclusions of Ag-bearing phases. Moreover, mean concentrations are typically in the same order of magnitude across samples from the same deposit. Băița Bihor is the exception, where means for individual samples within the deposit range from 545 (+/-47) to 14,928 (+/-1,673) ppm Ag.

Bismuth

Bismuth concentrations in galena vary significantly across the different deposits, both between different samples in a single deposit, and often between grains from a single sample. The lowest mean concentration for any sample was 0.06 ppm in sample DM3 (Vorța). This is in stark contrast to 36,453

ppm Bi recorded in BB55 (Băița Bihor), the highest measured mean concentration of any minor element in any sample analyzed here. Nevertheless, both the smooth LA-ICP-MS down-hole profiles and a low standard deviation on the mean in sample BB55 (11% relative) advocate that Bi is in solid solution. Individual analyses giving anomalous (wt.% level) Bi concentrations (excluded from the mean calculations in Table 2) were recorded in several samples: BdA 99-9 (Baia de Arieş); Hj13 (Herja); and 30 and 38 (Kochbulak). Micro-inclusions of Bi-bearing phases were interpreted as being responsible for these anomalous concentrations. Mean Bi concentrations vary by two orders of magnitude across the sample suites from Baia de Arieş, Băița Bihor, Herja and Kochbulak. Epithermal and skarn systems commonly display significant zoning of certain elements across and between ore zones as a response to temperature gradients. In the case of skarns, proximity to the source of ore-forming fluids is also considered to be a important factor (e.g., Meinert et al. 2005). Sample Hj13 from Herja contains galena that varies the most in Bi content, displaying concentrations ranging from 1.3 to 6,406 ppm. Despite the variation, this Bi is still interpreted as sitting in an atomic site within the galena crystal structure.

Antimony

Mean antimony concentrations in galena (Table 2) vary from 1.2 ppm in BB158 (Băița Bihor) to 3,518 ppm in Mo 11 (Mofjellet). On average the Herja samples contain the most Sb. Again, smooth LA-ICP-MS down-hole profiles and relative standard deviations averaging ~36% of the mean suggest the measured Sb is in solid solution. A single LA-ICP-MS spot in sample 47 (Kochbulak) returned an Sb concentration > 1 wt.% (not included in the mean, Table 2). Micro-inclusions of an Sb-bearing sulfide (likely tetrahedrite) were detected with the SEM in this sample. Sb shows far less variation across samples from a single deposit than Bi. Nevertheless, galena from both the Broken Hill and Băița Bihor sample suites displays variation up to two orders of magnitude, suggesting that some parts of these deposits are different to others, likely reflecting deposit-scale zoning. In the case of Băița Bihor,

this is readily interpreted in terms of higher Sb concentrations in samples from the Marta orepipe (distal to fluid source), relative to the Antoniu (proximal) orepipe. Relatively little spot-to-spot variation in Sb concentration is seen in most samples. Nevertheless, samples BH218 (Broken Hill; 4.7 to 161 ppm) and DMV99-22 (Vorța; 0.8 to 1519 ppm) both have standard deviations which exceed the mean.

Thallium

Thallium concentrations in galena vary over two orders of magnitude from 1.2 ppm in BH221 (Broken Hill) to 248 ppm in Bv-1 (Bleikvassli). Galena in the Bleikvassli samples is around four times more Tl-rich than in the Mt. Isa samples which contain the next most Tl-rich galena. However, typical Tl concentrations are <10 ppm in most deposits. Relative standard deviations of 20% (on average) and smooth LA-ICP-MS down-hole depth profiles indicate that Tl is in solid solution within galena. Thallium concentrations vary little within a single deposit, and are always less than one order of magnitude. A similar trend is present on the sample scale, with only BdA 99-9 (Baia de Arieş; 2.5 to 38.8 ppm) having a standard deviation greater than the mean.

Cadmium

Mean cadmium concentrations in galena also vary over two orders of magnitude across all analyzed samples. Most samples contain a few tens of ppm Cd, with mean concentrations ranging from 5.9 ppm in DMV99-22 (Vorța) up to the anomalously high value of 487 ppm in Mo 11 (Mofjellet). A few anomalously high Cd values were recorded in spot analyses from Mt. Isa, Bleikvassli and Kochbulak, resulting from the presence of micro-inclusions of Cd-bearing phases. Sub-micron-sized Cd-bearing phases were observed by SEM in sample 30 (Kochbulak), and are likely a Cd-rich variety in the tetrahedrite group. Apart from these anomalous analyses, all others recorded Cd in solid solution as evidenced by smooth LA-ICP-MS down-hole profiles and standard deviations averaging 36% of the mean. Cd concentrations are typically very uniform across all samples from a single deposit. Mofjellet

and Kochbulak are exceptions, showing concentration ranges in the respective sample suites from 18.4 to 487 ppm, and 10.1 to 145 ppm.

Copper

Considering the entire dataset, Cu concentrations in galena vary considerably from below mdl in 16 samples to as much as 797 ppm in DMV99-22 (Vorța). In some samples [Bv-97-3 (Bleikvassli), Mo 5 (Mofjellet), BB55, BBH16AB (Băița Bihor), T1a (Toroiaga) and 47 (Kochbulak)] irregular time-resolved down-hole profiles suggest the presence of sub-micron-scale inclusions of Cu-bearing minerals. Similar inclusions of Cu-bearing phases (likely of the tetrahedrite group) were also detected by SEM imaging in samples Mo 5, BBH16AB, T1a and 47. Despite these exceptions, the majority of analyses showing measurable Cu concentrations suggest that Cu is most likely in solid solution in the galena structure (smooth LA-ICP-MS down-hole profiles, standard deviations averaging 41% of the mean).

Selenium and tellurium

Both selenium and tellurium concentrations in galena vary extensively across the sample set (Table 2). For example, Se ranges from below the detection limit in 5 samples to 1,742 ppm in Bv-97-3 (Bleikvassli). Similarly, Te ranges from below the detection limit in 2 samples to 891 ppm in BB55 (Băița Bihor). While smooth LA-ICP-MS down-hole profiles infer that both elements can sit within the crystal lattice of galena, micro-inclusions of selenides are inferred in BH218, BH221 (Broken Hill), Kmi 2b (Kapp Mineral), BdA 99-9 (Baia de Arieş), BBH20 (Băița Bihor), TOR197 (Toroiaga) and ZN 99.2 (Zinkgruvan), while the presence of tellurides is inferred in 38 (Kochbulak). The concentrations of both elements can vary up to an order of magnitude within a set of samples from a single deposit, and in many cases vary significantly within a single sample (Table 2).

Indium and tin

Indium and tin were found to be present at detectable concentrations in most samples, but absolute values are typically <2 and <10 ppm respectively. In some cases galena appears to accommodate far more Sn in its structure, with 619 ppm Sn was recorded in Bv-97-3 (Bleikvassli), and each sample from this deposit returning over 100 ppm Sn. Neither In nor Sn vary significantly across samples from a single deposit.

Other elements

Minor amounts of gold (a few ppm), were measured within galena in a few samples (BdA99-5, BdA99-9, Kochbulak 47). Likewise, Kochbulak 30, BBH28A, and Mo11 contained low-ppm levels of Hg. Sub-micron-scale inclusions of Au- and Hg-bearing phases are likely responsible. Nevertheless, very low amounts of Au and Hg might theoretically be accommodated in the galena structure, although this cannot be proven by the present study. Chromium, Mn, Fe, Co, Ni, Zn, Ga, As, Mo and W could not be detected at measurable concentrations in any of the analyzed samples.

LA-ICP-MS mapping

Typifying either metamorphosed-recrystallized SEDEX (Bleikvassli; Fig. 5) or epithermal depositsa (Herja; Figs. 6 and 7, and Toroiaga; Fig. 8), LA-ICP-MS element maps of multi-component sulfide assemblages (galena + sphalerite ± chalcopyrite ± pyrite) show that in all cases Ag, Bi, Sb, Tl and Se are concentrated in galena. Tellurium is also present in epithermal galena. Sphalerite preferentially concentrates Cd, In, Hg and Ga, with Mn also present in epithermal sphalerite.

In the first map (Bleikvassli; Fig. 5), Ag is principally concentrated in galena; modest concentrations of Ag are also noted in sphalerite. Within the lateral resolution offered by the LA-ICP-MS maps, element maps display no compositional inhomogeneity in any of the sulfide minerals (limited by the 9 μm laser spot size and line spacings).

The first set of element maps of the galena-bearing assemblage (sample Hj13 from the Herja epithermal vein system (Fig. 6)), display the distribution of elements in a galena-sphalerite-chalcopyrite assemblage. This assemblage is interpreted as having crystallized at equilibrium due to the 120° triple junction between the three minerals. Silver, Sb, Bi, Tl, Te and Se are primarily contained within galena, whereas Cd, In, Sn and Co (as well as Mn, Hg and Ga, not shown on the figure), are predominantly concentrated in the coexisting sphalerite. Chalcopyrite is relatively barren of minor/trace elements but does contain minor amounts of In, Sn, Ag and Co. The relative concentrations of In, Sn and Co in the three sulfides are in the order Sp>Cp>Gn. Distributions of Bi, Se, Te, Sb, Ag and Tl display extensive heterogeneity within the galena. A systematic decrease in Bi, Se, Te, Ag and Tl is noted towards the mutual boundary with sphalerite. Increasing towards the boundary, Antimony displays an antithetic relationship compared to the other elements. The compositionally distinct zones in galena are cut perpendicularly at the galena-chalcopyrite boundary. Compositional zoning with respect to In and Sn is also noted in sphalerite.

A second set of element maps focusing on a single galena grain (sample Hj13 (Fig. 7)),, shows exemplary compositional zoning of various trace elements within galena. These maps show that the zonation is both oscillatory and sectorial, and that concentrations vary over as much as three orders of magnitude within the grain. Displaying comparable zonation patterns across the grain, Bi, Se, Ag, Te and Tl correlate with one another, with Sb behaving in an inverse manner. The sector zoning is seen particularly well on the Bi and Sb maps, with variation in concentration somewhat weaker than in the oscillatory zoning.

Figure 8 displays element maps of a four-component (galena-sphalerite-chalcopyrite-pyrite) assemblage from the Toroiaga epithermal vein system. Antimony, Bi, Ag, Tl, Te and Se are shown to be concentrated in galena. Manganese, Hg, Ga (not shown), Cd and In are chiefly concentrated within sphalerite, whereas Ni, Co, As, and Au (not shown) are almost exclusively present within pyrite. In striking contrast to the Herja maps (Figs. 6 and 7) where Sn is concentrated within sphalerite, Sn is

observed to be concentrated in chalcopyrite relative to co-existing minerals. Enclosed in chalcopyrite, the zoning in one galena grain is systematic (showing an Sb-rich core and Bi-rich rim). The second galena grain on the map displays a less clear pattern, marked by depletion in Bi towards the mutual boundary with sphalerite. This zoning pattern is mimicked by Se, Te, Tl and Ag, although for Te, Tl and Ag, this is not as well resolved on the figure. Again, Sb shows an antithetic relationship with Bi, with a Sb-enriched core and depleted rim in the galena crystal enclosed within chalcopyrite. Compositional zoning is also displayed in sphalerite (In), and in pyrite (Ni, As, Co and Au, not shown).

In the course of this study, we have generated a number of other LA-ICP-MS element maps on assemblages in the sample suite. Compositional zoning in galena has only been observed in sulfide assemblages of epithermal type, though rarely as spectacular as shown in Fig. 7.

DISCUSSION

Inter-element correlations

Considering the mean for each sample in the full dataset, Table 3 reveals a strong correlation (R^2 = 0.9645) between Ag and (Bi+Sb) in galena. This association is expected as a direct result of the coupled substitution $2Pb^{2+} \leftrightarrow Ag^{+} + (Bi, Sb)^{3+}$. In an ideal coupled substitution, mol.% Ag would be expected to equal mol.% (Bi+Sb). Adding both Cu and Tl to Ag increases the correlation with (Bi+Sb) to R^2 = 0.9662. Along with Ag both Cu and Tl likely exist in the +1 state in galena, and have been measured and are interpreted (based on limited intra-sample variance and smooth time-resolved down-hole spectra) as residing in solid solution in galena. These correlations indicate that both Cu and Tl may be involved in the same coupled substitution by which Ag^{+}, Bi^{3+} and Sb^{3+} are incorporated into the galena lattice. The coupled substitution may thus be more accurately expressed as $(Ag,Cu,Tl)^{+} + (Bi,Sb)^{3+} \leftrightarrow 2Pb^{2+}$.

Expressed as mol.% on binary plots (Fig. 9a-c), the fit to a 1:1 line is good for the epithermal and SEDEX groups, but in the case of the Băița Bihor skarn shows mol.% (Bi+Sb) exceeding mol.% (Ag+Cu+Tl) in which galena contains the highest Bi (Fig. 9c). Some other samples (e.g., Bleikvassli, Herja and Toroiaga) also display deviation from the 1:1 line at highest (Bi+Sb) values. Since all three elements are interpreted as being in solid solution, this implies more (Bi+Sb) is contained within the galena crystal lattice than the monovalent ions. This may imply that in environments significantly enriched in Bi and/or Sb, Bi^{3+} and/or Sb^{3+} can substitute into the crystal lattice of galena without a corresponding monovalent cation. In this event, the site usually filled by the monovalent cation would be left vacant, and the substitution would be $2(Bi, Sb)^{3+} + \square \leftrightarrow 3Pb^{2+}$. Although a structural configuration including vacancies is non-ideal (Silinsh 1980, Mishin et al. 2001), it may become acceptable when there are either not enough monovalent cations to substitute with Bi^{3+} and/or Sb^{3+}, or too much Bi and/or Sb to be accommodated solely via crystallization of coexisting minerals.

Indium and tin correlate strongly across the sample suite ($R^2 = 0.9169$, Table 3). This indicates that samples with galena rich in Sn are also rich in In, indicating that the availability of these elements in natural systems is intimately linked, perhaps from granite-sourced fluids. Tin however is typically present at concentrations 1-3 orders of magnitude higher than In (Fig. 9d). For galena rich in Sn (i.e., at Bleikvassli), it is interpreted that most of the Sn is partitioned into that mineral during syn-metamorphic recrystallization (see below) rather than incorporated within galena during initial crystallization. At lower ranges of concentration in the epithermal ores, correlation between In and Sn is weak (Fig. 9e).

Tellurium correlates strongly with both Ag and Bi ($R^2 = 0.7931$ and 0.8564, respectively; Table 3). However Figure 9f and 9g reveal that these correlations are only unambiguously expressed by the single skarn sampled (Băița Bihor). The presence of various bismuth chalcogenides of the tetradymite group is documented at Băița Bihor (Cioflica et al. 1995; Cioflica and Lupulescu 1995; Cioflica et al. 1997; Ilinca and Makovicky 1999; Cook et al. 2007; Ciobanu et al. 2011). It is possible that micro-

inclusions of Bi-tellurides were analyzed in the Băița Bihor samples, creating the impression that Bi and Te correlate in solid solution in galena. Furthermore, many of these Bi-tellurides can be significant carriers of Ag (15,626 ppm Ag recorded in tetradymite; Ciobanu et al. 2009), thus possibly creating an artificial secondary correlation between Ag and Te.

However, apparent correlation of Te with Bi and/or Ag at Băița Bihor (Fig. 9f, g) as a result of the presence of Ag-bearing Bi-telluride inclusions is not supported by the time-resolved LA-ICP-MS depth profiles. Figure 3a clearly shows smooth depth profiles for Bi, Ag and Te, strongly indicating that these elements are likely to occur in solid solution in galena at Băița Bihor. Bismuth-enriched galena is generally Ag-rich, arguably due to the coupled substitution $Ag^{+} + (Bi, Sb)^{3+} \leftrightarrow 2Pb^{2+}$.

Substitution mechanisms

Data obtained in this study supports coupled substitution mechanisms for Ag, Bi and Sb through the coupled substitution $Ag^{+} + (Bi,Sb)^{3+} \leftrightarrow 2Pb^{2+}$. When Bi and/or Sb are at high concentrations (~>2000 ppm), site vacancies may play a role through an additional substitution $2(Bi,Sb)^{3+} + \square \leftrightarrow 3Pb^{2+}$. Despite detection limits commonly as low as a few ppm, As is not detected in any significant concentrations in any sample, thus denying any confirmation that As^{3+} also takes part in the coupled substitution (Chutas et al. 2008).

Data introduced here suggest an expanded coupled substitution $(Ag,Cu,Tl)^{+} + (Bi,Sb)^{3+} \leftrightarrow 2Pb^{2+}$, i.e., also involving other monovalent cations. Since the oxidation state of Cu and Tl in galena cannot realistically be determined experimentally by EXAFS or XANES analysis due to the very low concentrations of these elements, the presence of Cu^{+} may only be assumed based on its presence in other common sulfide minerals such as chalcopyrite (Goh et al. 2006), or in Cu-In-substituted sphalerite (Cook et al. 2012). Thallium also prefers the +1 state over +3 as Tl^{3+} is a powerful oxidizing agent under normal conditions (Downs 1993). This study has also shown that far more Tl can be accommodated in galena than previously thought. The highest concentration of Tl in galena recorded in

this study (248 ppm; Bv-1, Bleikvassli) is an order of magnitude greater than the maximum 20 ppm reported by Nriagu (1998). Furthermore, contrary to Nriagu (1998) and Graham et al. (2009), galena appears to be the primary host for Tl in assemblages containing pyrite and sphalerite (Figs. 5-8). However it is unclear as to whether there is a systematic partitioning of Tl into galena in any sulfide ore.

It seems most likely that Cd and Hg are incorporated into galena via the simple bivalent cation substitution: $(Cd,Hg)^{2+} \leftrightarrow Pb^{2+}$. However this study has shown that the previously reported concentrations of Cd and Hg in solid solution in galena may be gross over-calculations. As Tauson et al. (2005) concluded, the 1.5 mol.% Cd reported by Tauson et al. (1986) is probably 1-2 orders of magnitude too high. The extent of the over-calculation of the Hg content of galena by Tauson et al. (1986) may be greater still, since only a few ppm Hg is recorded in galena in our study. Given the apparent lack of Hg in galena of our studied sample suite, partitioning of Hg between coexisting galena and sphalerite would not appear to be a prospective geothermometer for most deposits. Contrary to Bethke and Barton (1971), Mn has not been detected in galena in any significant concentrations or consistencies in any sample to permit its use as a geothermometer.

Although introduced as a possible mechanism for substitution of Sn into sphalerite (Cook et al. 2009b), incorporation of Sn in the +3 reduced state into galena via the coupled substitution $Ag^{+} + Sn^{3+} \leftrightarrow 2Zn^{2+}$ is not supported from the dataset. A trivalent state is also not the preferred oxidation state of Sn in minerals (Stwertka 1998). Rather, it is likely that Sn is being substituted into galena via $Sn^{4+} + \square \leftrightarrow 2Pb^{2+}$ involving the creation of vacancies, or potentially via simple bivalent cation substitution with Pb in the less stable +2 state: $Sn^{2+} \leftrightarrow Pb^{2+}$ (Stwertka 1998). To a limited extent, Sn could also be incorporated via $Sn^{4+} + 2(Ag,Cu,Tl)^{+} \leftrightarrow 3Pb^{2+}$, although the budget of monovalent cations is insufficient to incorporate the large concentrations of Sn documented in deposits such as Bleikvassli or Sullivan. In those most Sn rich galena specimens (e.g., Bv-97-3; Bleikvassli), it may be possible to determine the oxidation state of Sn in galena by XANES, EXAFS or XPS.

It can be assumed that In is incorporated in galena as a trivalent cation in the coupled substitution $Ag^{+} + (Bi,Sb,In)^{3+} \leftrightarrow 2Pb^{2+}$. Similarly, the data obtained in this study does not contradict the incorporation of both Se and Te through the substitution $(Se,Te)^{2-} \leftrightarrow S^{2-}$.

Grain-scale compositional zoning

Oscillatory zoning of minor/trace elements is documented in galena from two epithermal ores (Herja and Toroiaga; Figs. 6-8), confirming that like other sulfides, galena can be compositionally zoned at the grain-scale. Given the unmetamorphosed character of these geologically young (~10 Ma) deposits, zoning must have developed during initial crystallization. The 120° triple junctions between galena, sphalerite and chalcopyrite (Fig. 6) strongly suggest the sulfide assemblage at Herja formed at equilibrium, presumably during slow growth conditions. The zoning pattern shown by Sb is the reverse of that shown by Bi; when Bi is enriched in galena, Sb is depleted by necessity and *vice versa*. Silver, Tl, Se and Ag tend to follow Bi rather than Sb.

Various oscillatory zoning processes are debated in the wider literature (e.g., Ortoleva et al. 1987; Shore and Fowler 1996; L'Heureux 2013). By analogy with other minerals, the observed oscillatory zoning in galena can be interpreted either as an intrinsic or an extrinsic phenomenon, i.e., relating to crystal growth within a closed, local system, or involving chemical fluctuations in the ore-forming fluid. Considering that this phenomenon is only observed here in galena from epithermal veins, it is possible that the zoning relates to crystallization in a locally closed system within the larger, open hydrothermal system. Such conditions would be readily attained by pooling of fluid within vein cavities. It appears that syn-metamorphic, open system crystallization does not allow for the development of compositional zoning in such a way, but could lead to zoning via extrinsic mechanisms.

Reeder and Grams (1987) proposed a model for sector zoning in crystals growing from an aqueous solution as a result of differential partitioning between non-equivalent crystal faces. Shore and Fowler

(1996) claim this model may be applicable to oscillatory zoning as well, since both types of zoning are often visible in the same crystal as observed in this study. Indeed, oscillatory zoning was replicated by Reeder et al. (1990) in synthetic calcite without changing the composition of an isothermal solution.

The absence of grain-scale zoning in the other samples may suggest that such phenomena are rarely preserved, and that in particular recrystallized galena will not show zoning. Including the possible role of defects and twinning, identifying the relationships between crystal zoning and lattice-scale structural features would be a worthy topic for future study. This could be accomplished via a combination of focused-ion-beam (FIB)-SEM and transmission electron microscopy methods as was applied to sphalerite and other sulfides (Ciobanu et al. 2011).

Sharp et al. (1990) show the importance of nanoscale features in galena. Using scanning tunneling microscopy (STM) they were able to identify defects in the surface structure of Ag-Sb-bearing galena. The study described a distortion in the surface structure of Ag- and Sb-bearing galena, resulting in kinking of atomic rows that parallel [110]. This distortion is interpreted as the result of strain in the atomic structure caused by the grouping of substituted Ag and Sb in the galena lattice. If true, this may indicate that substituted elements (especially Ag and Sb) in the galena lattice are not evenly distributed, but clustered.

Partitioning between galena and co-existing sulfides

A number of samples in this study (Table 1) contain coexisting sphalerite which has also been analyzed by LA-ICP-MS in previous studies (Cook et al. 2009b; Lockington et al. in revision). This permits a comparison of minor/trace element partitioning trends among coexisting sulfides, even if equilibrium crystallization is not necessarily implied.

Silver, Sb and Bi are primarily contained within galena whereas Cd, In and Hg are concentrated in sphalerite. Tin is largely absent in sphalerite, where only the Bleikvassli samples have concentrations of Sn significantly above mdl. In coexisting galena, concentrations range from 0.7 ppm (Mo 5, Mofjellet)

to 595 ppm (V538, Bleikvassli), with galena always containing more Sn than sphalerite. It has been suggested above that galena becomes the primary host of Sn in a recrystallized assemblage. Nevertheless, galena still contains more Sn than sphalerite even in SEDEX (Mt. Isa) and epithermal (Toroiaga) ores. This study thus clearly shows that the role played by galena in controlling trace Sn distributions may be significantly greater than previously recognized. However, further work to establish this would need to consider the role played by coexisting chalcopyrite which is generally considered a good Sn-carrier (e.g., Kase 1987).

Our data shows that Tl is always primarily concentrated in galena, with only the Mt. Isa sphalerite containing concentrations of Tl above mdl. This again suggests that galena is the primary host of Tl in base metal ores, contrary to Nriagu (1998) and Graham et al. (2009). Copper concentrations are always an order of magnitude greater in sphalerite than coexisting galena, indicating that sphalerite is the preferred host. Sample Mo 5 (Mofjellet) is the exception with 12 ppm Cu recorded in galena compared to 8 ppm Cu in the sphalerite. Selenium is essentially absent from sphalerite whenever coexisting with galena. Galena can be relatively Se-rich (concentrations up to 553 ppm Se in Bv-1, Bleikvassli) suggesting that in a galena-sphalerite assemblage, Se is preferentially partitioned into galena.

The data presented here represent an important step towards our ongoing goal of quantifying $X_{sphalerite}/X_{galena}$, $X_{sphalerite}/X_{chalcopyrite}$, and $X_{chalcopyrite}/X_{galena}$ ratios, where X is any given trace element.

IMPLICATIONS

The element maps in this study (Figs. 5-8) reveal several ore genesis-related aspects of trace element incorporation in certain multi-component sulfide assemblages. Mutual grain relationships in these samples suggest co-crystallization of base metal sulfides (excluding pyrite), either via co-precipitation (epithermal, skarn), or during syn-metamorphic re-crystallization at amphibolite facies or above (some SEDEX deposits included in this study). Galena is the better host for Ag, Tl, Bi, Sb and Se, whereas

Cd, In, Hg and Mn are systematically enriched in co-existing sphalerite. This is seen across the dataset despite the wide range of absolute concentrations and diverse character of the sample suite. The correlation of mono- and trivalent ions in galena is readily related to the substitution mechanism $(Ag,Cu,Tl)^{1+} + (Bi, Sb)^{3+} \leftrightarrow 2Pb^{2+}$.

Broadly, concentrations of Sb in galena are higher in SEDEX and epithermal systems than in skarn. Galena from Băița Bihor is 5 times richer in Bi than in any other deposit analyzed (Table 2, Fig. 4). This is primarily due to the anomalous Bi-rich environment of this deposit, in which a wide range of rare Bi-sulfosalt minerals are documented. We also note enrichment of Te in galena from epithermal/skarn systems but not in SEDEX deposits (Fig. 4).

The behavior of Sn in multi-component sulfide assemblages shows differences. Tin is clearly enriched in galena from SEDEX ores, and conversely incorporated in sphalerite or chalcopyrite in some epithermal systems (Fig. 4). This may be seen as a peculiarity of SEDEX systems, where despite their age, geological setting or metamorphic overprint, local variation of Sn seems dependent upon the presence or absence of chalcopyrite. The LA-ICP-MS element maps from Bleikvassli (Fig. 5) suggest that the degree of syn-metamorphic recrystallization may also play a role. In this case recrystallized galena is highly enriched in Sn, while the coexisting sphalerite that arguably formed in equilibrium with the galena is almost entirely depleted in the element. Tin is commonly a minor component in sphalerite (Stoiber 1940; Cook et al. 2009b; Ye et al. 2011), and since sphalerite is abundant in the Bleikvassli samples, it can be inferred that recrystallization of a coexisting galena-sphalerite assemblage at upper amphibolite facies conditions results in re-partitioning of Sn from sphalerite to galena. However, Tin-bearing galena is not exclusive to recrystallized SEDEX deposits. Although metamorphosed to lower amphibolite facies, galena from Sullivan also contains over 400 ppm Snwith no evidence for any significant recrystallization of the sulfide assemblage. Chalcopyrite may also be a primary host for Sn. This is seen in the LA-ICP-MS element maps for the Toroiaga sample (Fig. 8). Contrasting with those in Figs. 6 and 7, these distributions suggest that the Toroiaga assemblage may

not represent equilibrium crystallization (telescoping of earlier Cu-rich and later Zn-Pb-rich sulfide assemblages?). Alternatively, it may suggest that the partitioning of Sn among co-existing sulfides depends on temperature or other parameters.

Although beyond the scope of the present study, the partitioning behavior of Sn between coexisting sulfides under hydrothermal/metamorphic conditions represents a significant research gap that needs to be assessed in terms of the galena-sphalerite-chalcopyrite ternary assemblage.

The contrasting behavior of Sn in the two metallogenically-related epithermal systems (Figs. 6-8) is notable, as it highlights not only the potential for development of new geothermo(baro)meters based on the partitioning of a given element into a mineral pair, or of two elements between two minerals (e.g., Sn and Cd in galena and sphalerite), but also for geochemical tools in metallogenetic studies and exploration vectoring.

The samples covered in this study derive from deposits that were formed in a range of different geodynamic environments and crystallized over a wide range of pressure-temperature conditions. Despite this, our results suggest a communality of element behavior. One clear finding is the greater compositional variance in samples from epithermal deposits relative to the metamorphosed systems. Absolute element concentrations are also dependent on the source of elements in each setting, whether it be leaching from the sedimentary pile in the case of the SEDEX systems, or magmatic sources in epithermal deposits. This would logically explain the relative enrichments in elements such as Sn and Bi in the two groups.

Trace element concentrations and their grain-scale distributions in galena could also be used to identify spatial and/or temporal trends within individual metallogenic belts. In addition they could represent markers of processes of ore formation, as well informing us on deposits that have undergone superimposed metamorphism and deformation. Trace element data for specific minerals can also guide optimization of ore processing (especially where extraction of valuable trace/minor elements is sought), and assist in recognition of potential mechanisms for retention and release of hazardous elements in

galena within a mine stockpile or tailings heap. Lastly, we also see potential for using galena trace element geochemistry for trace/minor element vector approaches in mineral exploration, notably for recognition of proximal-to-distal trends within a given ore system. Additional data are needed to substantiate and expand on many of our findings. In particular, data from other sulfide systems will help elucidate mechanisms of substitution, contribute towards establishing partitioning relationships in multi-component assemblages, and further resolve the critical issue of solid solution vs. fine-scale inclusions for some elements. We hope our findings will catalyze further studies of galena.

ACKNOWLEDGMENTS

Aoife McFadden and Ken Neubauer (Adelaide Microscopy) are thanked for support with analysis. The authors express their gratitude to the numerous individuals, without whom access to many of the samples analyzed here would not have been possible. We appreciate constructive comments from three anonymous *American Mineralogist* reviewers and Editor Paul Tomascak, which have helped us to improve this manuscript. This is TRaX contribution no. 290.

REFERENCES CITED

Amcoff, O. (1976) The solubility of silver and antimony in galena. Neues Jahrbuch für Mineralogie Monatshefte, (6), 247-261.

Balić-Zunić, T., and Bente, K. (1995) The two polymorphs of $TlPbSbS_3$ and the structural relations of phases in the system $TlSbS_2$-PbS. Mineralogy and Petrology, 53, 265-276.

Bethke, P.M., and Barton, P.B. (1971) Distribution of some minor elements between coexisting sulfide minerals. Economic Geology, 66, 140-163.

Billay, A.Y., Kisters, A.F.M., Meyer, F.M., and Schneider, J. (1997) The geology of the Lega Dembi gold deposit, southern Ethiopia: implications for Pan-African gold exploration. Mineralium Deposita, 32, 491-504.

Bjerkgard, T., Marker, M., Sandstad, J., Cook, N.J., and Sørdahl, T. (2001) Ore potential with emphasis on gold in the Mofjellet Deposit, Rana, Nordland, Norway. Norges geologiske Undersøkelse Report 2001.050.

Blackburn, W.H. and Schwendeman, J.F. (1977) Trace element substitution in galena. Canadian Mineralogist, 15, 365-377.

Borcoş, M., Lang, B., Bostinescu, S., and Gheorghita, I. (1975) Neogene hydrothermal ore deposits in the volcanic Gutai Mountains, part III. Revue Roumaine de Géologie, Géophysique, Géographie, Serie Géologie, 19, 21-35.

Chouinard, A., Paquette, J., and Williams-Jones, A.E. (2005) Crystallographic controls on trace-element incorporation in auriferous pyrite from the Pascua epithermal high-sulfidation deposit, Chile–Argentina. Canadian Mineralogist, 43, 951-963.

Chutas, N.I., Kress, V.C., Ghiorso, M.S., and Sack, R.O. (2008) A solution model for high-temperature PbS-$AgSbS_2$-$AgBiS_2$ galena. American Mineralogist, 93, 1630-1640.

Ciobanu, C.L., Cook, N.J., and Ivascanu, P. (2001) Ore deposits of the Vorța–Dealul Mare area, South Apuseni Mts., Romania: textures and a revised genetic model. ABCD-Geode 2001. Romanian Journal of Mineral Deposits, 79, 46-47.

Ciobanu, C.L., Cook, N.J. and Stein, H. (2002) Regional setting and geochronology of the Late Cretaceous Banatitic Magmatic and Metallogenic Belt. Mineralium Deposita, 37, 541-567.

Ciobanu, C.L., Gabudeanu, B., and Cook, N.J. (2004) Neogene ore deposits and metallogeny of the Golden Quadrilateral, South Apuseni Mountains, Romania. In: C.L. Ciobanu and N.J. Cook, Eds., Gold-Silver-Telluride Deposits of the Golden Quadrilateral, South Apuseni Mts., Romania. Guidebook, International Field Workshop of IGCP-486, Alba Iulia, Romania, 31st August – 7th September 2004. IAGOD Guidebook Series, 12, p. 221-225.

Ciobanu, C.L., Cook, N.J., Pring, A., Brugger, J., Danyushevsky, L.V., and Shimizu, M. (2009) 'Invisible gold' in bismuth chalcogenides. Geochimica et Cosmochimica Acta, 73, 1970-1999.

Ciobanu, C.L., Cook, N.J., Utsunomiya, S., Pring, A., and Green, L. (2011) Focussed ion beam–transmission electron microscopy applications in ore mineralogy: Bridging micro- and nanoscale observations. Ore Geology Reviews, 42, 6-31.

Ciobanu, C.L., Cook, N.J., Kelson, C.R., Guerin, R., Kalleske, N., and Danyushevsky, L. (2013) Trace element heterogeneity in molybdenite fingerprints stages of mineralization. Chemical Geology, 347, 175-189.

Ciobanu, C.L., Brugger, J., Cook, N.J., Mills, S., Elliot, P., Damian, G., and Damian, F. (2014) Grațianite, $MnBi_2S_4$, a new mineral from the Băița Bihor skarn, Romania. American Mineralogist, 99, 1163-1170.

Cioflica, G., Vlad, S., Volanschi, E., and Stoici, S. (1977) Magnesian skarns and associated mineralization at Băița Bihor. Studii şi Cercetare Géologie Géofizică şi Géographie, Serie Géologie, 22, 39-57.

Cioflica, G., Jude, R., Lupulescu, M., Simon, G., and Damian, G. (1995) New data on the Bi-minerals from the mineralizations related to Palaeocene magmatites in Romania. Romanian Journal of Mineralogy, 76, 9-23.

Cioflica, G., Lupulescu, M., and Shimizu, M. (1997) Bismuth minerals from the Băița Bihor and Valisor-Tincova Mines: New compositional data. Romanian Journal of Mineralogy, 78, 13-14.

Cioflica, G., Jude, R., Berbeleac, I., Lupulescu, M., Costea, D., and Costea, A. (1999) Epithermal gold mineralizations of low-sulfidation type from Baia de Aries Mine, Southern Apuseni Mountains, Romania. Revue Roumaine de Géologie, 43, 3-18.

Coleman, R. (1959) New occurrences of ferroselite ($FeSe_2$). Geochimica et Cosmochimica Acta, 16, 296-301.

Cook, N.J. (1993) Conditions of metamorphism estimated from alteration lithologies and ore at the Bleikvassli Zn-Pb-(Cu) deposit, Nordland, Norway. Norsk geologisk tidsskrift, 73, 226-233.

Cook, N.J. (1997) Bismuth and bismuth-antimony sulphosalts from Neogene vein mineralisation, Baia Borsa area, Maramures, Romania. Mineralogical Magazine, 61, 387-409.

Cook, N.J. (2001) Ore mineralogical investigation of the Mofjell deposit (Mo i Rana, Nordland, Norway) with emphasis on gold and silver distribution. Norges geologiske undersøkelse Report 2001.051, 31 pp.

Cook, N.J., and Ciobanu, C. (2001) Gold sulphosalt and telluride mineralogy of the Lega Dembi shear zone hosted gold deposit, Ethiopia. In: Piestrzynski A. et al., Eds., Mineral Deposits at the Beginning of the 21st Century, Swets and Zeitlinger Publishers, Lisse, p 719-722.

Cook, N.J. and Ciobanu, C.L. (2003) Cervelleite, Ag_4TeS, from three localities in Romania, substitution of Cu, and the occurrence of the associated phase, Ag_2Cu_2TeS. Neues Jahrbuch für Mineralogie Monatshefte, 321-336.

Cook, N.J., and Damian, G.S. (1997) New data on “plumosite” and other sulphosalt minerals from the Herja hydrothermal vein deposit, Baia Mare district, Rumania. Geologica Carpathica, 48, 387-399.

Cook, N.J., Spry, P.G., and Vokes, F.M. (1998) Mineralogy and textural relationships among sulphosalts and related minerals in the Bleikvassli Zn-Pb-(Cu) deposit, Nordland, Norway. Mineralium Deposita, 34, 35-56.

Cook, N.J., Ciobanu, C.L., Wagner, T., and Stanley, C.J. (2007) Minerals of the system Bi–Te–Se–S related to the tetradymite archetype: review of classification and compositional variation. Canadian Mineralogist, 45, 665-708.

Cook, N.J., Ciobanu, C.L., and Mao, J.W. (2009a) Textural control on gold distribution in As-free pyrite from the Dongping, Huangtuliang and Hougou gold deposits, North China Craton, (Hebei Province, China). Chemical Geology, 264, 101-121.

Cook, N.J., Ciobanu, C.L., Pring, A., Skinner, W., Shimizu, M., Danyushevsky, L., Saini-Eidukat, B., and Melcher, F. (2009b) Trace and minor elements in sphalerite: A LA-ICPMS study. Geochimica et Cosmochimica Acta, 73, 4761-4791.

Cook, N.J., Ciobanu, C.L., Spry, P.G., Voudouris, P. and the participants of IGCP-486 (2009c) Understanding gold-(silver)-telluride-(selenide) deposits. Episodes, 32, 249-263.

Cook, N.J., Ciobanu, C.L., Danyushevsky, L.V., and Gilbert, S. (2011) Minor and trace elements in bornite and associated Cu–(Fe)-sulfides: A LA-ICP-MS study. Geochimica et Cosmochimica Acta, 75, 6473-6496.

Cook, N.J., Ciobanu, C.L., Brugger, J., Etschmann, B., Howard, D.L., de Jonge, M.D., Ryan, C.G., and Paterson, D.J. (2012) Determination of the oxidation state of Cu in substituted Cu-In-Fe-bearing sphalerite via μ-XANES spectroscopy. American Mineralogist, 97, 476-479.

Cook, N.J., Ciobanu, C.L., Giles, D., and Wade B. (2013a) Correlating textures and trace elements in ore minerals. Mineral deposit research for a high-tech world. Proceedings, 12th Biennial SGA Meeting, 12-15 August 2013, Uppsala, Sweden, p. 288-291.

Cook, N.J., Ciobanu, C.L., Meria, D., Silcock, D., and Wade, B. (2013b) Arsenopyrite-pyrite association in an orogenic gold ore: tracing mineralization history from textures and trace elements. Economic Geology, 108, 1273–1283.

Costagliola, P., Di Benedetto, F., Benvenuti, M., Bernardini, G.P., Cipriani, C., Lattanzi, P.F., and Romanelli, M. (2003) Chemical speciation of Ag in galena by EPR spectroscopy. American Mineralogist, 88, 1345-1350.

Danyushevsky, L., Robinson, P., Gilbert, S., Norman, M., Large, R., McGoldrick, P., Shelley, M. (2011) Routine quantitative multi-element analysis of sulphide minerals by laser ablation ICP-MS: Standard development and consideration of matrix effects. Geochemistry Exploration Environment Analysis, 11, 51-60.

Darrow, M.S., White, W.B., and Roy, R. (1966) Phase relations in the system PbS-PbTe. Transactions, Metallurgical Society of AIME, 236, 654-658.

De Paoli, G.R., and Pattison, D.R.M. (2000) Thermobarometric calculation of peak metamorphic conditions of the Sullivan deposit. In J.W. Lydon, T. Hoy, J.F. Slack, and M.E. Knapp, Eds., The Geological Environment of the Sullivan Deposit, British Columbia. Geological Association of Canada, Mineral Deposits Division, Special Publication no. 1, p. 272-280.

Di Benedetto, F., Bernardini, G.P., Costagliola, P., Plant, D., and Vaughan, D.J. (2005) Compositional zoning in sphalerite crystals. American Mineralogist, 90, 1384-1392.

Downs, A.J. (1993) Chemistry of aluminium, gallium, indium, and thallium. Springer, 526 pp.

Dragov, P., and Petrunov, R. (1996) Elazite porphyry copper-precious metals (Au and PGE) deposit. Proceedings, Annual Meeting of IGCP Project 356, Sofia, Bulgaria, p. 171-175.

Fiori, M., Garbarino, C., Grillo, S., Solomon, T., and Valera, R. (1988) Mineral paragenesis in the Au-Ag-Cu-Zn-Pb-Te deposit of Lega Dembi (Ethiopia). Proceedings, Bicentennial Gold, Melbourne, Australia, p. 184-186.

Flood, B. (1967) Sulphide mineralizations within the Hecla Hoek complex in Vestspitsbergen and Bjørnøya. Norsk Polarinstitutt Årbok, 1967, 109-127.

Foord, E.E., and Shawe, D.R. (1989) The Pb-Bi-Ag-Cu-(Hg) chemistry of galena and some associated sulfosalts; a review and some new data from Colorado, California and Pennsylvania. Canadian Mineralogist, 27, 363-382.

Foord, E.E., Shawe, D.R., and Conklin, N.M. (1988) Coexisting galena, PbS_{ss} and sulfosalts: evidence for multiple episodes of mineralization in the Round Mountain and Manhattan gold districts, Nevada. Canadian Mineralogist, 26, 355-376.

Georgiev, G. (2008) A genetic model of the Elatsite porphyry copper deposit, Bulgaria. Geochemistry, Mineralogy and Petrology, 46, 143-160.

Ghițulescu, T.P. and Socolescu, M. (1941) Étude géologique et miniére des Monts Metalliféres (Quadrilatère aurifère et régions environnantes). Anuarul Institutului de Geologie, 21, 181–464.

Ghosal, S. and Sack, R.O. (1999) Bi-Sb Energetics in Sulfosalts and Sulfides. Mineralogical Magazine, 63, 723-733.

Giuli, G., Paris, E., Wu, Z., De Panfilis, S., Pratesi, G., and Cipriani, C. (2005) The structural role of Ag in galena (PbS). A XANES study. Physica Scripta, T115, 387-389.

Goh, S.W., Buckley, A.N., Lamb, R.N., Rosenberg, R.A., and Moran, D. (2006) The oxidation states of copper and iron in mineral sulfides, and the oxides formed on initial exposure of chalcopyrite and bornite to air. Geochimica et Cosmochimica Acta, 70, 2210-2228.

Graham, G.E., Kelley, K.D., Slack, J.F., and Koenig, A.E. (2009) Trace elements in Zn–Pb–Ag deposits and related stream sediments, Brooks Range Alaska, with implications for Tl as a pathfinder element. Geochemistry: Exploration, Environment, Analysis, 9, 19-37.

Hamilton, J., Bishop, D., Morris, H., and Owens, O. (1982) Geology of the Sullivan orebody, Kimberley, BC, Canada. In: Hutchinson, R.W. Spence, C.D., and Franklin, J.M. Eds., Precambrian Sulphide Deposits. Geological Association of Canada, Special Paper 25, p, 597-665.

Haydon, R.C., and McConachy, G.W. (1987) The stratigraphic setting of Pb-Zn-Ag mineralization at Broken Hill. Economic Geology, 82, 826-856.

Hedström, P., Simeonov, A., and Malmstrom, L. (1989) The Zinkgruvan ore deposit, south-central Sweden; a Proterozoic, proximal Zn-Pb-Ag deposit in distal volcanic facies. Economic Geology, 84, 1235-1261.

Hoda, S.N. and Chang, L.L.Y. (1975) Phase relations in the systems $PbS-Ag_2S-Sb_2S_3$ and $PbS-Ag_2S-Bi_2S_3$. American Mineralogist, 60, 621-633.

Hinchey, J.G., Wilton, D.H.C., and Tubrett, M.N. (2003) A LAM–ICP–MS Study of the Distribution of Gold in arsenopyrite from the Lodestar Prospect, Newfoundland, Canada. Canadian Mineralogist, 41, 353-364.

Ilinca, G., and Makovicky, E. (1999) Bismuth sulphotellurides in the Banatitic Province, Romania. Mineralogy in the System of Earth Sciences, Abstract volume, University of Bucharest, 40-41.

Ilinca, G., Makovicky, E., Topa, D., and Zagler, G. (2012) Cuproneyite, $Cu_7Pb_{27}Bi_{25}S_{68}$, a new mineral species from Băița Bihor, Romania. Canadian Mineralogist, 50, 353-370.

Ingham, E.S., Cook, N.J., Cliff, J., Ciobanu, C.L., and Huddleston, A. (2014) A combined chemical, isotopic and microstructural study of pyrite from roll-front uranium deposits, Lake Eyre Basin, South Australia. Geochimica et Cosmochimica Acta, 125, 440-465.

Islamov, F., Kremenetsky, E., Minzer, E., and Koneev, R. (1999) The Kochbulak - Kairagach ore field. In T. Shayakubov, F. Islamov, A. Kremenetshy and R. Seltmann Eds., Au, Ag, and Cu Deposits of Uzbekistan; Excursion Guidebook; International Field Conference of IGCP-373, Joint SGA-IAGOD symposium, Excursion B6, IGCP-SGA-IAGOD.

Jeppsson, M.L. (1989) Mineral chemistry of silver in antimony and bismuth rich sulphide ore in Bergslagen, central Sweden. Neues Jahrbuch für Mineralogie Monatshefte, 205-216.

Kase, K. (1987) Tin-bearing chalcopyrite from the Izumo vein, Toyoha mine, Hokkaido, Japan. Canadian Mineralogist, 25, 9-13.

Knipe, S.W., Foster, R.P., and Stanley, C.J. (1992) Role of sulphide surfaces in sorption of precious metals from hydrothermal fluids. Transactions, Institution of Mining and Metallurgy, B101, 83-88.

Kovalenker, V., Safonov, Y., Naumov, V., and Rusinov, V. (1997) The epithermal gold-telluride Kochbulak deposit (Uzbekistan). Geology of Ore Deposits, 39, 107-128.

Krismer, M., Vavtar, F., Tropper, P., Sartory, B., and Kaindl, R. (2011) Mineralogy, mineral chemistry anpetrology of the Ag-bearing Cu-Fe-Pb-Zn sulfide mineralizations of the Pfunderer Berg (South Tyrol, Italy). Austrian Journal of Earth Sciences, 104, 36-48.

Lang, B. (1979) The base metals-gold hydrothermal ore deposits of Baia Mare, Romania. Economic Geology, 74, 1336-1351.

Large, R.R., Danyushevsky, L., Hollit, C., Maslennikov, V., Meffre, S., Gilbert, S., Bull, S., Scott, R., Emsbo, P., Thomas, H., Singh, B., and Foster, J. (2009) Gold and Trace Element Zonation in Pyrite Using a Laser Imaging Technique: Implications for the Timing of Gold in Orogenic and Carlin-Style Sediment-Hosted Deposits. Economic Geology, 104, 635-668.

Larocque, A.C.L., Jackman, J.A., Cabri, L.J., and Hodgson, C.J. (1995) Calibration of the ion microprobe for the determination of silver in pyrite and chalcopyrite from the Mobrun VMS deposit, Rouyn-Noranda, Quebec. Canadian Mineralogist, 33, 361-372.

L'Heureux, I. (2013) Self-organized rhythmic patterns in geochemical systems. Philosophical Transactions of the Royal Society A371, doi: 10.1098/rsta.2012.0356.

Liu, H., and Chang, L.L.Y. (1994) Phase relations in the system PbS-PbSe-PbTe. Mineralogical Magazine, 58, 567-578.

Lockington, J.A., Cook, N.J. and Ciobanu, C.L. (accepted, in revision) Trace and minor elements in sphalerite from metamorphosed sulphide deposits. Mineralogy and Petrology.

Lueth, V.W., Megaw, P.K.M., Pingitore, N.E., and Goodell, P.C. (2000) Systematic Variation in Galena Solid-Solution Compositions at Santa Eulalia, Chihuahua, Mexico. Economic Geology, 95, 1673-1687.

Lydon, J.W. (2000) A synopsis of the current understanding of the geological environment of the Sullivan deposit. In: Lydon, J.W., Höy, T., Slack, J.F., and Knapp, M.E., Eds., The Geological Environment of the Sullivan Deposit, British Columbia. Geological Association of Canada, Mineral Deposits Division, Special Publication 1, p. 12-31.

Mathias, B., and Clark, G. (1975) Mount Isa copper and silver-lead-zinc orebodies—Isa and Hilton mines. In: Knight, C.L., Ed., Economic Geology of Australia and Papua New Guinea vol. 1, AusIMM, p. 351-372.

Meinert, L.D., Dipple, G.M., and Nicolescu, S. (2005) World skarn deposits. Economic Geology 100th Anniversary Volume, p. 299–336.

Mishin, Y., Mehl, M., Papaconstantopoulos, D., Voter, A., and Kress, J. (2001) Structural stability and lattice defects in copper: ab initio, tight-binding, and embedded-atom calculations. Physical Review, B63, 224106.

Morey, A.A., Tomkins, A.G., Bierlein, F.P., Weinberg, R.F., and Davidson, G.J. (2008) Bimodal distribution of gold in pyrite and arsenopyrite: Examples from the Archean Boorara and Bardoc Shear Systems, Yilgarn Craton, Western Australia. Economic Geology, 103, 599-614.

Müller, W., Shelley, M., Miller, P., and Broude, S. (2009) Initial performance metrics of a new custom-designed ArF excimer LA-ICPMS system coupled to a two-volume laser-ablation cell. Journal of Analytical Atomic Spectrometry, 24, 209-214.

Neubauer, N., Lips, A., Kouzmanov, K., Lexa, J. and Ivaşcanu, P. (2005) Subduction, slab detachment and mineralization: The Neogene in the Apusenu Mountains and Carpathians. Ore Geology Reviews, 27, 13-44.

Nriagu, J.O. (1998) Thallium in the Environment. Advances in Environmental Science and Technology, vol. 29. Wiley and Sons, New York, 284 p.

Ortoleva, P.J., Merino, E., Moore, C., and Chadam, J. (1987a) Geochemical self-organization: I. Reaction-transport feedbacks and modeling approach. American Journal of Science, 287, 979-1007.

Painter, M.G.M., Golding, S.D., Hannan, K.W., and Neudert, M.K. (1999) Sedimentologic, petrographic, and sulfur isotope constraints on fine-grained pyrite formation at Mount Isa Mine and environs, Northwest Queensland, Australia. Economic Geology, 94, 883-912.

Parr, J., and Plimer, I. (1993) Models for Broken Hill-type lead-zinc-silver deposits. Mineral deposits modeling. Geological Association of Canada Special Paper 40, 245-288.

Paton, C., Hellstrom, J., Paul, B., Woodhead, J., and Hergt, J. (2011) Iolite: Freeware for the visualisation and processing of mass spectrometric data. Journal of Analytical Atomic Spectrometry, 26, 2508-2518.

Perkins, W. (1997) Mount Isa lead-zinc orebodies: Replacement lodes in a zoned syndeformational copper-lead-zinc system? Ore Geology Reviews, 12, 61-110.

Plimer, I.R. (2007) The world's largest Zn-Pb-Ag deposit: a re-evaluation of Broken Hill (Australia). In: Andrew, C.J., Ed., Mineral Deposits: Digging Deeper. Irish Association for Economic Geology, Dublin, p. 1239-1242.

Plotinskaya, O.Y., Kovalenker, V., Seltmann, R., and Stanley, C. (2006) Te and Se mineralogy of the high-sulfidation Kochbulak and Kairagach epithermal gold telluride deposits (Kurama Ridge, Middle Tien Shan, Uzbekistan). Mineralogy and Petrology, 87, 187-207.

Pring, A., and Williams, T.B. (1994) A HRTEM study of defects in silver-doped galena. Mineralogical Magazine, 58, 455-459.

Ramdohr, P. (1980) The Ore Minerals and their Intergrowths, 2nd edition. Pergamon Press, 1207 p.

Reeder, R.J., Fagioli, R.O., and Meyers, W.J. (1990) Oscillatory zoning of Mn in solution-grown calcite crystals. Earth-Science Reviews, 29, 39-46.

Reeder, R.J., and Grams, J.C. (1987) Sector zoning in calcite cement crystals: Implications for trace element distributions in carbonates. Geochimica et Cosmochimica Acta, 51, 187-194.

Reich, M., Palacios, C., Barra, F., and Chryssoulis, S. (2013) “Invisible” silver in chalcopyrite and bornite from the Mantos Blancos Cu deposit, northern Chile. European Journal of Mineralogy, 25, 453-460.

Renock, D., and Becker, U. (2011) A first principles study of coupled substitution in galena. Ore Geology Reviews, 42, 71-83.

Rosenberg, J.L., Spry, P.G., Jacobson, C.E., Cook, N.J., and Vokes, F.M. (1998) Thermobarometry of the Bleikvassli Zn-Pb-(Cu) deposit, Nordland, Norway. Mineralium Deposita, 34, 19-34.

Saager, R. (1967) Drei Typen von Kieslagerstätten im Mofjell-Gebiet, Nordland, und ein neuer Vorschlag zur Gliederung der Kaledonischen Kieslager Norwegens. Norsk geologisk tidsskrift, 47, 333-358.

Scaini, M.J., Bancroft, G.M., and Knipe, S.W. (1997) An XPS, AES, and SEM study of the interactions of gold and silver chloride species with PbS and FeS_2: Comparison to natural samples. Geochimica et Cosmochimica Acta, 61, 1223-1231.

Sharp, T.G., and Buseck, P.R. (1993) The distribution of Ag and Sb in galena; inclusions versus solid solution. American Mineralogist, 78, 85-95.

Sharp, T.G., Zheng, N.J., Tsong, I.S., and Buseck, P.R. (1990) Scanning tunneling microscopy of defects in Ag- and Sb-bearing galena. American Mineralogist, 75, 1438-1442.

Shore, M., and Fowler, A.D. (1996) Oscillatory zoning in minerals; a common phenomenon. Canadian Mineralogist, 34, 1111-1126.

Silinsh, E.A. (1980) Role of Structural Defects in the Formation of Local Electronic States in Molecular Crystals. In Organic Molecular Crystals, Springer Series in Solid-State Sciences, p. 139-222.

Spry, P.G., Plimer, I.R., and Teale, G.S. (2008) Did the giant Broken Hill (Australia) Zn–Pb–Ag deposit melt? Ore Geology Reviews, 34, 223-241.

Stoiber, R.E. (1940) Minor elements in sphalerite. Economic Geology, 35, 501-519.

Stwertka, A. (1998) "Tin". Guide to the Elements, revised edition. Oxford University Press.

Szoke, A., and Steclaci, L. (1962) Regiunea Toroiaga- Baia Borsa. Studiu Geologic, Petrografic, Mineralogic si Geochimic. Editura Academiei Republicii Populare Romine, Bucharest, 240 pp.

Tauson, V.L., Paradina, L.F., and Andrulaitis, L.D. (1986) The entry of mercury into galena and the new galena-sphalerite geothermometer. Geochemistry International, 23, 55-61.

Tauson, V.L., Parkhomenko, I.Y., Babkin, D.N., Men'shikov, V.I., and Lustenberg, E.E. (2005) Cadmium and mercury uptake by galena crystals under hydrothermal growth: A spectroscopic and element thermo-release atomic absorption study. European Journal of Mineralogy, 17, 599-610.

Van Achterberg, E., Ryan, C.G., Jackson, S.E., and Griffin, W.L. (2001) Data reduction software for LAICP-MS. In: Sylvester J.P. Ed., Laser-ablation-ICPMS in the Earth Sciences; Principles and Applications. Mineralogical Association of Canada, Short Course Series 29, p. 239-243.

Van Hook, H.J. (1960) The ternary system Ag_2S-Bi_2S_3-PbS. Economic Geology, 55, 759-788.

Vlad, Ş. and Borcoş, M. (1997) Alpine metallogenesis of the Romanian Carpathians. Romanian Journal of Mineral Deposits, 78, 5-20.

Vokes, F.M. (1963) Geological studies on the Caledonian pyritic zinc-lead orebody at Bleikvassli, Norland, Norway. Norges geologiske Undersøkelse, 222, 1-126.

Vokes, F.M. (1966) On the possible modes of origin of the Caledonian sulfide ore deposit at Bleikvassli, Nordland, Norway. Economic Geology, 61, 1130-1139.

Wernick, J.H. (1960) Constitution of the $AgSbS_2$-PbS, $AgBiS_2$-PbS, and $AgBiS_2$-$AgBiSe_2$ systems. American Mineralogist, 45, 591–598.

Wilson, S.A. (1997) The collection, preparation, and testing of USGS reference material BCR-2, Columbia River, Basalt. U.S.G.S. Open File Report, 98-00x.

Wilson, S.A., Ridley, W.I., and Koenig, A.E. 2002. Development of sulfide calibration standards for the laser ablation inductively-coupled plasma mass spectrometry technique. Journal of Analytical Atomic Spectrometry, 17, 406-409.

Winderbaum, L., Ciobanu, C.L., Cook, N.J., Paul, M., Metcalfe, A. and Gilbert, S. (2012) Multivariate analysis of an LA-ICP-MS trace element dataset for pyrite. Mathematical Geosciences, 44, 823-842.

Ye, L., Cook, N.J., Ciobanu, C.L., Liu, Y.P., Zhang, Q., Gao, W., Yang, Y.L., and Danyushevsky, L.V. (2011) Trace and minor elements in sphalerite from base metal deposits in South China: a LA-ICPMS study. Ore Geology Reviews, 39, 188-217.

FIGURE CAPTIONS

FIGURE 1. Sketch World map showing approximate locations of deposits sampled in this study. BMMB – Banatitic Magmatic and Metallogenetic Belt; BM – Baia Mare; GQ – Golden Quadrilateral; SAM – South Apseni Mts.

FIGURE 2. Reflected light photomicrographs illustrating various occurrences of, and textures in, galena. (a) Typical perfect cubic cleavage on [001] parting on [111] in galena (Gn) (Băița Bihor, BBH20). (b) Common triangular cleavage pits on polished surface of galena (Kapp Mineral, Kmi 4). (c) Galena as a matrix for various gangue and ore minerals (Mt. Isa, 5984B C1). Sp: sphalerite, Py: pyrite). (d) Galena and sphalerite filling the matrix between idioblastic pyrite (Bleikvassli, V538). (e) Intergrown galena and sphalerite from a massive SEDEX ore (Zinkgruvan, ZN 99.2) and (f) banded galena, sphalerite and pyrrhotite (Po) in a layered SEDEX ore (Sullivan).

FIGURE 3. Representative time-resolved LA-ICP-MS depth profiles for galena. Parts-per-million concentrations are given for selected elements. CPS = counts-per-second. (a) Flat spectra reflecting solid solution for Bi, Ag, Tl, Te, Cd and Cu (BBH20, Băița Bihor). (b) Flat spectra for Bi, Ag, Sb, Tl and Sn (Bv-97-3, Bleikvassli). (c) Peak on Zn profile indicating mineral inclusion. Note flat spectra for Sn and In (V538, Bleikvassli). (d) Peak on Au profile indicating inclusion (BdA 99-5, Baia de Arieş). (e) Parallel peaks on Sb, Hg and Cd profiles reflecting mineral inclusions (30, Kochbulak). (f) Peak on Ag and Sb profiles reflecting mineral inclusion. Concentrations are calculated by selecting and integrating only the signal before the peak (BH218, Broken Hill).

FIGURE 4. Cumulative plots showing the mean concentrations with standard deviations for Bi, Sb, Ag, Tl, Sn, Cd, Te and Se in galena from each sample (see Table 2). The data are arranged in order of increasing element abundance within each sample in each deposit type (as for Bi, top left). Individual samples may appear in different positions for different elements. The reader is referred to Table 2 for raw values.

FIGURE 5. LA-ICP-MS element maps (S, Pb, Zn, Ag, Bi, Sb, Sn, Tl, Se, In, Cd, Hg) of a massive sulfide assemblage comprising co-existing galena (Gn), sphalerite (Sp) and pyrite (Py) (Bv-1, Bleikvassli). Note the preferential concentration of Bi, Sb, Sn, Tl and Se in galena, and of In, Cd and Hg in sphalerite, and also

modest enrichment of Ag in galena relative to sphalerite. Gallium (not shown) is also preferentially incorporated in sphalerite. Scales in ppm.

FIGURE 6. LA-ICP-MS element maps (S, Fe, Pb, Ag, Sb, Bi, Tl, Te, Se, Cu, Zn, Cd, In, Sn, Co) of an equilibrium assemblage comprising co-existing galena (Gn), sphalerite (Sp) and chalcopyrite (Cp) (Hj13, Herja). Note the preferential concentration of Ag, Sb, Bi, Tl, Te and Se in galena, and of Cd, In, Sn and Co in sphalerite. Note also compositional zoning of all elements in galena, and of In (and to some extent Sn), in sphalerite. Relative concentrations of In, Sn and Co in the three sulfides are in the order Sp>Cp>Gn. Silver and Sb are also noted within fractures at or close to the chalcopyrite-sphalerite contact. Manganese, Hg and Ga (not shown) are also preferentially incorporated in sphalerite. Scales in ppm.

FIGURE 7. LA-ICP-MS element maps (S, Pb, Sb, Bi, Ag, Se, Te and Tl) of assemblage comprising co-existing galena (Gn), sphalerite (Sp) and chalcopyrite (Cp) (Hj13, Herja), with emphasis on oscillatory and sectorial compositional zoning in galena; see text for further explanation. Scales in ppm.

FIGURE 8. LA-ICP-MS element maps (Fe, Pb, Cu, Sb, Bi, Ag, Tl, Te, Se, Cd, Sn, In) of assemblage comprising co-existing galena (Gn), sphalerite (Sp), chalcopyrite (Cp) and pyrite (Py) (Emeric2, Toroiaga). See text for further explanation. Scales in ppm.

FIGURE 9. Binary plots showing inter-element correlations (mol.% basis). (a-c) (Ag+Cu+Tl) vs. (Bi+Sb) in galena from VHMS/SEDEX, epithermal and skarn ores, respectively. Dashed line: ideal 1:1 correlation. (d-e) In vs. Sn in galena from SEDEX and epithermal ores, respectively. Dashed line: ideal 1:1 correlation. (d-e) In vs. Sn in galena from SEDEX and epithermal ores, respectively. (f) Te vs. Bi, and (g) Te vs. Ag in galena. Lines of best fit and R^2 values are given.

Table 1. Summary of deposits from which galena has been sampled in this study

Deposit/Type	Conditions of formation or metamorphism	References	Samples	Ore mineralogy	Textures (% sulphides)
Broken Hill, Australia SEDEX (metamorphosed, equilibrium co-crystallization)	Granulite facies (750-800°C, 5-6 kbar)	Haydon & McConachy (1987), Parr & Plimer (1993), Plimer (2007), Spry et al. (2008)	BH218* BH221* BH233	Gn-Sp-Py-Cp-Po Gn-Sp-Cp-Py-Po Gn-Sp-Py-Cp-Po	massive (>85) massive (>85) massive (70)
Mt. Isa, Australia SEDEX or replacement-type (Py earlier than BMS)	Greenschist facies	Mathias & Clark (1975), Perkins (1997), Painter et al. (1999)	5984B C1* 5984B C2* 5990 C1	Gn-Sp-Py-Cp Sp-Py-Gn-Cp Gn-Py-Sp-Cp	massive (70) massive (50) banded (50)
Elatsite, Bulgaria Porphyry Cu	Various assemblages deposited at 190-575 °C	Dragov & Petrunov (1996), Georgiev (2008)	ELS-157	Sp-Gn-Cp-Py	Massive (50)
Sullivan, Canada Giant SEDEX	Upper greenschist (450 °C, 3.8 kbar)	Hamilton et al. (1982), De Paoli & Pattison (2000), Lydon (2000)	Sul-1	Gn-Sp-Po	Banded (85)
Lega Dembi, Ethiopia Orogenic gold, Adola greenstone belt	Amphibolite facies (430-520 °C)	Fiori et al. (1988), Billay et al. (1997), Cook & Ciobanu (2001)	7011A	Cp-Gn-Sp	Massive (75)
Bleikvassli, Norway SEDEX (metamorphosed, equilibrium co-crystallization)	Upper amphibolite - lower granulite facies (570 °C, 7.5-8.0 kbar)	Vokes (1963, 1966), Cook (1993), Cook et al. (1998), Rosenberg et al. (1998)	Bv-1* Bv-97-3 V57-852 V446* V538*	Py-Sp-Gn-Po-Cp Gn-Sp-Po Cp-Py-Gn-Sp-Po Po-Py-Sp-Cp-Gn-Tet Py-Sp-Gn-Po-Cp-Tet	massive (>85) massive (80) massive (>85) massive (70) massive (70)
Kapp Mineral, Norway SEDEX	Very weakly metamorphosed	Flood (1967)	Kmi 2b Kmi 4	Gn Gn-Cp	semi-massive (50) semi-massive (40)
Mofjellet, Norway SEDEX (metamorphosed, equilibrium co-crystallization)	Amphibolite facies (550 °C, 7.0 kbar ?)	Saager (1967), Bjerkgård et al. (2001), Cook (2001)	Mo 2* Mo 5* Mo 11	Py-Gn-Sp-Cp-Po Sp-Cp-Py-Po-Gn-Tet Gn-Py-Sp	semi-massive (50) semi-massive (35) massive (75)
Baia de Aries, Romania Epithermal system (Pb-Zn orepipe)	Formed at < ~300 °C	Cioflica et al. (1999), Ciobanu et al. (2004)	BdA 99-1 BdA 99-5 BdA 99-9	Py-Sp-Gn-Cp Py-Gn-Sp-Cp Sp-Py-Gn-Cp	massive (>85) massive (>85) semi-massive (30)
Baita Bihor, Romania Polymetallic Skarn (BB55, BB158, BBH16AB, BBH16B, BBH20, BBH25: Antoniu orepipe; BBH28A, BBH32: Marta orepipe)	Formed at ~500 °C (proximal), ~375 °C (distal)	Cioflica et al. (1977), Shimizu et al. (1995), Ciobanu et al. (2002)	BB55 BB158 BBH16AB BBH16B BBH20 BBH25 BBH28A BBH32	Gn-Sp Gn-Sp-Cp Gn-(Cp,Tet) Gn-Sp-Cp Gn-Sp-Cp Sp-Gn-Cp Gn-Cp-Sp Sp-Gn-Py-Cp	minor (5) minor (10) massive (70) massive (50) semi-massive (40) semi-massive (20) semi-massive (40) semi-massive (25)
Herja, Romania Epithermal Zn-Pb-Ag-Au vein system (Py earlier than BMS)	Formed at < ~300 °C	Borcos et al. (1975), Lang (1979), Cook & Damian (1997)	Hj13 Hj14	Gn-Cp-Py-Tet-Sp-Po Gn-Sp	massive (>85) semi-massive (35)
Toroiaga, Romania Epithermal Zn-Pb-Ag-Au veins (Py predates BMS which are in equilibrium)	Formed at ~350 °C	Szoke & Steclaci (1962), Gotz et al. (1990), Cook (1997)	Emeric2 T1a** TOR197	Py-Cp-Gn-Sp Py-Cp-Sp-Gn Py-Sp-Cp-Gn	massive (85) massive (75) massive (75)
Vorta, Romania VMS deposit (ophiolite sequence)	Formed at 250-300 °C	Ciobanu et al. (2001)	DM3 DMV99-22	Gn-Cp-Py-Sp Sp-Cp-Py-Gn	massive (60) massive (60)
Zinkgruvan, Sweden SEDEX	Upper amphibolite facies	Billström (1985), Hedström et al. (1989)	ZN 99.2	Sp-Gn-Cp	massive (>85)
Kochbulak, Uzbekistan Epithermal (Py earlier than BMS)	Formed at 200-400 °C	Kovalenker et al. (1997), Islamov et al. (1999), Plotinskaya et al. (2006)	30 38 47	Gn-Tet-Py-Sp-Cp Cp-Gn-Tet-Sp-Py Gn-Sp-Cp-Py-Tet	vein (15) semi-massive (25) semi-massive (30)

Mineral abbreviations: BMS – base metal sulphides; Cp - chalcopyrite; Gn - galena; Po - pyrrhotite; Py - pyrite; Sp - sphalerite; Tet -tetrahedrite-tennantite.

* coexisting sphalerite analysed in Lockington et al. (in revision), ** in Cook et al. (2009b).

Table 2. Summary of minor/trace element concentrations in galena determined by LA-ICP-MS. Data in ppm.

LOCALITY	SAMPLE	Cu	Se	Ag	Cd	In	Sn	Sb	Te	Au	Hg	Tl	Bi
Broken Hill	**BH218**												
Australia	**Mean (24)**	1.7	207	96	11	0.24	83	28	4.5	0.44	0.34	1.3	79
	S.D.	0.37	246	66	4.7	0.06	6.1	39	0.10	-	0.06	0.16	6.5
	Min.	1.3	47	40	5.2	0.15	70	4.7	4.4	0.44	0.27	1.1	65
	Max.	2.2	821	271	22	0.36	94	161	4.6	0.44	0.38	1.8	97
	BH221												
	Mean (23)	2.2	104	386	32	0.37	122	198	2.5	0.45	0.37	1.2	36
	S.D.	0.69	60	125	11	0.07	13	83	-	-	0.09	0.11	2.5
	Min.	1.4	21	177	11	0.23	104	64	2.5	0.45	0.28	1.0	30
	Max.	3.2	161	663	56	0.51	152	405	2.5	0.45	0.45	1.4	41
	BH233												
	Mean (24)	<97	118	652	16	0.16	51	973	0.87	0.03	0.44	2.5	172
	S.D.	-	97	74	4.9	0.06	3.5	110	0.39	0.01	0.07	0.21	12
	Min.	<44	49	484	10	0.08	45	745	0.49	0.01	0.39	2.1	148
	Max.	<97	186	777	28	0.31	61	1127	1.5	0.05	0.49	2.9	196
Mt Isa	**5984B C1**												
Australia	**Mean (12)**	3.3	<149	870	8.0	0.67	5.8	1200	<5.4	<0.47	0.63	48	27
	S.D.	2.0	-	94	1.3	0.71	0.79	130	-	-	0.29	4.9	2.1
	Min.	1.9	<74	693	5.8	0.16	3.8	964	<3.7	<0.33	0.42	37	22
	Max.	6.1	<149	1056	10	1.2	6.8	1454	<5.4	<0.47	0.83	55	29
	5984B C2												
	Mean (11)	1.6	<94	810	6.5	<0.11	6.0	1164	<3.1	<0.38	0.38	35	20
	S.D.	0.28	-	75	1.0	-	2.6	113	-	-	0.03	3.1	1.2
	Min.	1.2	<75	655	5.2	<0.08	3.9	888	<2.3	<0.25	0.36	28	19
	Max.	1.8	<94	949	8.0	<0.11	12.9	1262	<3.1	<0.38	0.41	39	22
	5990 C1												
	MEAN (24)	<183	79	1521	12	0.05	4.8	1904	1.1	0.02	0.75	29	13
	S.D.	-	69	320	3.2	0.03	1.8	394	0.47	0.01	0.28	1.3	0.77
	Min.	<85	30	1117	5.5	0.02	2.7	1489	0.74	0.02	0.55	27	12
	Max.	<183	128	2355	19	0.10	11.1	3032	1.8	0.04	0.94	32	16
Elatsite	**ELS-157**												
Bulgaria	**Mean (24)**	<442	146	618	29	0.05	<6.0	13	143	0.09	<1.2	3.1	1388
	S.D.	-	97	385	14	0.02	-	13	44	0.07	-	0.28	913
	Min.	<196	60	124	7.6	0.03	<2.7	1.4	45	0.02	<0.64	2.5	82.3
	Max.	<442	314	1452	64	0.08	<6.0	54	228	0.26	<1.2	3.6	3255
Sullivan	**Sullivan**												
Canada	**Mean (24)**	25	<291	805	28	1.3	404	1109	0.25	0.01	0.41	11.9	5.1
	S.D.	5.0	-	129	6.8	0.28	92	154	0.11	0.01	-	0.92	1.2
	Min.	22	<75	499	15	0.65	255	743	0.12	<0.01	0.41	9.9	4.0
	Max.	29	<291	974	38	1.6	528	1326	0.45	0.02	0.41	13.5	9.2
Lega	**7011 A**												
Dembi	**Mean (24)**	45	148	188	99	0.02	<2.3	97	28	0.04	0.72	1.7	3.1
Ethiopia	**S.D.**	15	-	29	30	<0.01	-	9.5	6.0	0.03	-	0.20	4.9
	Min.	34	148	129	52	0.02	<1.4	81	17	0.01	0.72	1.4	0.18
	Max.	56	148	237	220	0.03	<2.3	117	41	0.09	0.72	2.1	17
Bleikvassli	**Bv-1**												
Norway	**Mean (24)**	<423	553	1214	11	1.0	346	1171	2.2	0.07	<1.2	248	1158

	S.D.	-	289	156	6.0	0.34	112	240	0.77	0.07	-	26	55
	Min.	<262	348	871	2.6	0.42	76	668	1.4	0.03	<0.78	159	993
	Max.	<423	757	1475	25.7	1.9	610	1738	3.7	0.21	<1.2	289	1249
	Bv-97-3												
	Mean (24)	<788	1742	1439	46	1.9	619	896	3.2	0.06	<1.8	113	2697
	S.D.	-	1238	172	18	0.45	70	355	1.5	0.02	-	5.3	123
	Min.	<267	48	1118	24	0.94	501	355	1.2	0.04	<0.80	102	2507
	Max.	<788	3006	1968	98	2.9	757	1870	6.0	0.10	<1.8	122	2931
	V446												
	Mean (12)	5.4	208	1176	8.1	0.84	283	476	5.5	0.47	0.62	108	2468
	S.D.	2.9	43	106	2.0	0.15	48.4	131	1.4	-	0.12	6.1	134
	Min.	2.5	155	1017	5.7	0.53	179	266	4.1	0.47	0.53	96	2157
	Max.	12	304	1318	12	1.0	343	705	7.7	0.47	0.70	123	2657
	V538												
	Mean (12)	5.4	153	1464	12.1	1.8	595	1659	6.4	<0.71	<0.61	170	1224
	S.D.	2.0	51	236	4.6	0.39	126	435	1.4	-	-	18.2	79
	Min.	2.2	94	1124	6.3	1.0	374	1026	5.1	<0.41	<0.44	139	1087
	Max.	8.9	243	1796	20	2.3	764	2439	7.9	<0.71	<0.61	201	1341
	V57-852												
	Mean (12)	150	170	1204	33	0.45	139	494	8.9	0.01	0.24	158	3278
	S.D.	127	108	108	9.4	0.07	16	240	2.1	<0.01	0.04	15.9	89
	Min.	14.9	43.3	1005	7.7	0.32	115	104	4.7	0.01	0.21	137	3086
	Max.	309	387	1380	50	0.57	168	1160	13	0.02	0.27	190	3476
Kapp Mineral Norway	**Kmi 2b**												
	Mean (24)	3.8	259	125	9.0	0.09	3.6	120	2.1	0.05	0.51	1.9	10
	S.D.	1.2	278	42	3.2	0.05	3.1	19	0.78	0.01	0.29	1.0	9.5
	Min.	1.6	86	79	2.7	0.04	1.3	71	1.5	0.04	0.30	0.68	1.4
	Max.	5.7	580	238	18	0.16	7.9	147	3.0	0.07	0.71	3.2	38
	Kmi 4												
	Mean (24)	<198	722	223	11	0.05	4.3	250	1.2	0.03	1.0	1.8	16
	S.D.	-	-	41	3.2	0.02	0.83	42	0.66	0.01	-	0.21	8.2
	Min.	<72	722	138	7.7	0.03	3.8	160	0.59	0.02	1.0	1.5	2.3
	Max.	<198	722	286	20.9	0.07	4.9	316	2.2	0.06	1.0	2.2	30
Mofjellet Norway	**Mo 2**												
	Mean (23)	2.5	28	1151	42	0.10	1.1	1450	30	0.29	0.35	1.3	172
	S.D.	1.1	11	174	27	-	0.23	440	6.1	0.01	0.09	0.17	16
	Min.	1.3	15	760	15	0.10	0.91	759	20	0.28	0.25	1.0	135
	Max.	4.5	48	1490	137	0.10	1.5	2445	39	0.29	0.43	1.6	202
	Mo 5												
	Mean (12)	12	318	1531	18	<0.11	0.73	2309	52	<0.47	0.43	1.5	296
	S.D.	7.8	37.3	301	14	-	-	826	5.3	-	-	0.09	13
	Min.	2.1	277	985	8.2	<0.09	0.73	1032	40	<0.36	0.43	1.3	268
	Max.	24	377	2032	48	<0.11	0.73	4271	60	<0.47	0.43	1.6	308
	Mo 11												
	Mean (24)	13	582	2981	487	0.06	1.1	3518	48	0.37	1.2	1.5	141
	S.D.	5.0	546	918	137	0.02	0.31	1151	7.5	0.89	0.89	0.17	4.2
	Min.	8.2	192	1612	261	0.03	0.72	1814	31	<0.01	0.39	1.2	136
	Max.	20	2674	4713	826	0.11	1.8	5630	64	2.2	4.7	1.8	151
Baia de Aries Romania	**BdA 99-1**												
	Mean (11)	<253	-	414	54	0.06	<6.3	445	168	0.12	<1.2	4.0	66
	S.D.	-	-	37	11	0.03	-	42	166	0.06	-	1.9	56
	Min.	<162	-	348	35	0.04	<4.4	375	14	0.05	<0.87	2.4	13

	Max.	<253	-	474	70	0.07	<6.3	522	439	0.17	<1.2	7.7	161
	BdA 99-5												
	Mean (24)	<74	316	503	49	0.10	<3.3	528	123	0.40	0.47	3.1	9.6
	S.D.	-	269	132	6.9	0.01	-	172	140	0.61	0.08	2.5	10
	Min.	<14	125	304	39	0.09	<1.7	276	6.3	0.01	0.37	1.5	0.11
	Max.	<74	506	826	70	0.11	<3.3	983	469	2.2	0.56	14	36
	BdA 99-9												
	Mean (12)	<108	287	1114	44	0.08	<3.7	355	43	2.2	0.55	9.0	1680
	S.D.	-	68	486	9.6	0.05	-	168	26	4.9	-	10	1302
	Min.	<69	239	605	27	0.02	<2.6	148	13	0.02	0.55	2.5	41
	Max.	<108	334	2194	62	0.15	<3.7	781	103	11	0.55	39	4379
Baita Bihor Romania	**BB55**												
	Mean (11)	215	-	14928	113	0.07	3.9	10	891	0.43	0.58	37	36453
	S.D.	22	-	1673	30	0.05	0.72	2.7	143	0.23	0.02	2.6	4047
	Min.	199	-	10679	64	0.03	3.1	6.2	575	0.13	0.57	33	26544
	Max.	230	-	16763	166	0.12	4.6	14	1030	0.82	0.60	42	41040
	BB158												
	Mean (12)	282	7.3	6057	48	0.04	<3.2	1.2	351	0.19	0.64	69	18079
	S.D.	58	-	721	28	0.02	-	0.83	46	0.18	0.09	14	528
	Min.	198	7.3	4423	12	0.03	<2.3	0.13	271	0.02	0.56	42	17161
	Max.	352	7.3	7100	101	0.05	<3.2	2.4	415	0.60	0.73	93	18759
	BBH16AB												
	Mean (24)	57	198	4528	103	0.01	1.2	14	226	0.31	0.33	21	11155
	S.D.	17	62	225	44	0.01	-	13	26	0.38	0.05	3.1	810
	Min.	42	91	4086	34	0.01	1.2	0.31	183	<0.01	0.29	15	9565
	Max.	74	309	5061	174	0.02	1.2	42	269	1.2	0.38	25	13110
	BBH16B												
	Mean (24)	<232	456	827	57	0.07	<3.7	2.7	197	0.08	<1.1	9.0	2168
	S.D.	-	421	154	19	0.06	-	2.5	32	0.05	-	2.1	457
	Min.	<119	159	675	21	0.03	<2.4	0.35	137	0.02	<0.65	6.9	1797
	Max.	<232	754	1459	98	0.15	<3.7	9.1	260	0.18	<1.1	16	4023
	BBH20												
	Mean (24)	54	173	2820	89	0.02	1.1	14	260	0.02	0.16	21	7978
	S.D.	25	103	171	21	0.01	0.29	5.9	30	0.01	0.02	4.4	228
	Min.	15	64	2568	54	0.01	0.59	7.3	212	<0.1	0.11	14	7554
	Max.	109	483	3192	130	0.02	1.7	33	340	0.06	0.18	30	8329
	BBH25												
	Mean (12)	30	157	545	67	0.01	<0.74	225	65	0.02	0.22	10	918
	S.D.	9.1	43	47	9.4	-	-	28	27	0.01	0.04	1.0	116
	Min.	20	78	486	45	0.01	<0.61	180	42	<0.01	0.17	7.8	821
	Max.	44	231	659	77	0.01	<0.74	261	128	0.03	0.28	11.6	1246
	BBH28A												
	Mean (24)	<502	34	697	199	0.15	3.8	301	192	0.06	1.4	13.9	1168
	S.D.	-	11	94	27	0.08	-	60	71	0.05	0.49	6.1	216
	Min.	<136	26	474	153	0.03	3.8	150	72	0.03	0.64	3.0	597
	Max.	<502	42	827	251	0.29	3.8	392	323	0.17	2.6	24	1404
	BBH32												
	Mean (12)	<29	609	3775	65	0.01	1.0	31	314	0.04	0.22	15	9209
	S.D.	-	183	182	12	<0.01	0.20	6.8	18	0.02	0.06	1.0	343
	Min.	<19	420	3475	30	0.01	0.77	14	292	0.01	0.17	13	8677
	Max.	<29	1018	4125	76	0.01	1.2	39	352	0.06	0.29	17	10038
Herja	***Hj13**												

Romania	**Mean (24)**	42	712	1896	21	0.05	2.8	1901	19	0.02	<0.90	2.5	1054
	S.D.	16	642	414	3.6	0.04	1.0	625	25	<0.01	-	1.0	1864
	Min.	31	45	1014	15	0.01	1.9	511	0.35	0.02	<0.45	1.7	1.3
	Max.	53	1352	2964	28	0.14	4.9	2873	97	0.02	<0.90	6.6	6406
	***Hj14**												
	Mean (24)	<273	165	2778	17	0.06	5.4	3257	3.6	0.05	<1.2	4.6	9.1
	S.D.	-	85	586	3.8	0.02	1.4	689	3.0	0.03	-	0.86	14
	Min.	<166	46	1769	10	0.03	4.1	2173	1.1	0.02	<0.71	3.3	0.17
	Max.	<273	234	3899	24	0.09	8.0	4630	9.3	0.13	<1.2	6.2	46
Toroiaga	***Emeric2**												
Romania	**Mean (23)**	<295	153	3055	71	0.09	4.9	2370	149	0.05	1.1	4.6	2248
	S.D.	-	87	422	20	0.07	1.3	352	50	0.02	0.23	1.7	902
	Min.	<162	49	2587	34	0.03	2.6	1834	81	0.03	0.93	3.1	822
	Max.	<295	276	4047	100	0.21	7.3	3090	269	0.09	1.3	10.6	4544
	T1a												
	Mean (24)	345	195	3141	75	0.17	4.1	2192	181	0.11	0.81	3.5	2680
	S.D.	-	61	473	14	0.10	0.72	410	77	0.17	0.25	1.1	811
	Min.	345	117	2259	50	0.03	3.2	1267	70	0.02	0.53	1.8	1687
	Max.	345	352	4172	99	0.33	5.1	3058	436	0.59	1.1	6.5	4644
	TOR197												
	Mean (12)	296	32	1185	78	0.15	5.5	1274	24	0.03	0.79	2.4	238
	S.D.	-	28	124	16	0.04	1.1	105	9.4	0.01	-	0.26	168
	Min.	296	9.6	998	51	0.09	3.8	1038	12	0.03	0.79	2.0	47
	Max.	296	63	1345	103	0.21	6.9	1403	45	0.05	0.79	2.9	566
Vorta	**DM3**												
Romania	**Mean (24)**	43	32	274	29	0.01	<0.93	252	6.1	0.05	0.27	2.1	0.06
	S.D.	11	-	61	15	<0.01	-	80	2.0	0.03	0.03	0.09	0.01
	Min.	36	32	73	1.3	<0.01	<0.69	23	3.5	0.01	0.24	2.0	0.04
	Max.	51	32	359	51	0.02	<0.93	363	12	0.14	0.30	2.3	0.08
	DMV99-22												
	Mean (24)	797	252	134	5.9	0.04	2.3	352	13	0.03	0.70	2.8	0.67
	S.D.	616	95	64	3.4	0.01	-	404	7.4	0.01	-	0.09	1.5
	Min.	145	164	59	0.67	0.03	2.3	0.80	1.7	0.02	0.70	2.6	0.12
	Max.	2184	352	326	12	0.06	2.3	1519	27	0.06	0.70	2.9	5.6
Zinkgruvan	**ZN 99.2**												
Sweden	**Mean (24)**	<20	36	676	14	0.04	4.5	721	0.34	0.02	<0.79	1.6	1.7
	S.D.	-	30	60	2.2	-	0.64	38	0.13	0.01	-	0.14	0.13
	Min.	<7.7	8.6	578	10	0.04	3.0	659	0.21	0.01	<0.23	1.5	1.4
	Max.	<20	95	771	18	0.04	5.3	781	0.50	0.03	<0.79	2.1	1.9
Kochbulak	**30**												
Uzbekistan	**Mean (23)**	191	140	320	10	0.09	1.0	550	31	0.14	2.1	2.8	172
	S.D.	152	69	95	11	0.14	-	345	9.2	0.09	3.0	0.23	171
	Min.	69	57	125	3.6	0.01	1.0	38	1.9	0.01	0.20	2.3	6.8
	Max.	455	218	502	51	0.38	1.0	781	47	0.38	7.4	3.1	632
	38												
	Mean (12)	550	56	307	19	0.11	2.8	683	14	0.17	0.36	3.0	76
	S.D.	178	57	126	19	0.10	-	487	24	0.15	0.28	0.57	74
	Min.	344	5.9	100	3.3	0.02	2.8	102	0.32	0.01	0.19	2.3	0.09
	Max.	831	118	529	66	0.25	2.8	1572	79	0.42	0.86	4.6	211
	47												
	Mean (24)	214	189	523	145	0.60	1.7	951	103	0.65	1.0	4.8	0.77
	S.D.	139	194	196	78	0.50	0.79	344	117	1.0	0.81	1.1	1.2

Min.	92	12	31	2.6	0.02	0.82	25.6	0.33	0.06	0.28	2.4	0.07
Max.	693	491	776	250	1.7	3.7	1633	474	3.9	2.1	6.0	4.8

* Galena grains analysed are zoned.
(X) Number of individual spot analyses on that sample.
- insufficient data for calculation.
All <mdl values excluded from statistical calculations; numbers with < in the table were all less than mdl.
The number given is the average mdl within that population.

Table 3. Correlation table of minor and trace elements in galena.

R^2	Cu	Se	Ag	Cd	In	Sn	Sb	Te	Au	Hg	Tl	Bi	(Sb+Bi)
Cu	1.000	0.031	0.013	0.002	0.021	0.036	0.007	0.014	0.005	0.032	0.010	0.022	0.020
Se		1.000	0.003	0.012	0.153	0.185	0.007	0.012	0.000	0.019	0.066	0.004	0.003
Ag			1.000	0.061	0.010	0.007	0.000	**0.793**	0.004	0.000	0.001	**0.905**	**0.965**
Cd				1.000	0.017	0.027	0.088	0.063	0.016	0.132	0.022	0.019	0.034
In					1.000	**0.917**	0.012	0.054	0.006	0.036	0.433	0.010	0.008
Sn						1.000	0.006	0.051	0.011	0.059	0.466	0.006	0.004
Sb							1.000	0.082	0.022	0.005	0.000	0.083	0.024
Te								1.000	0.010	0.001	0.001	**0.856**	**0.835**
Au									1.000	0.010	0.008	0.008	0.005
Hg										1.000	0.069	0.001	0.000
Tl											1.000	0.018	0.019
Bi												1.000	**0.981**
(Sb+Bi)													1.000

Correlation coefficients (R^2) calculated from the mean concentration of each minor/trace element pair in each sample.


Kapp Mineral (Hecla Hoek Complex, Svalbard, Late Proterozoic/Paleozoic)
Bleikvassli, Mojfellet (Caledonides, Paleozoic)
Zinkgruvan (Bergslagen, Early Proterozoic)
Herja, Toroiaga (BM, Neogene)
Baia de Aries(GQ, Neogene)
Elatsite (BMMB, Late Cretaceous)
Baita Bihor (BMMB, Late Cretaceous)
Vorta (SAM, Jurrasic ophiolite)
Sullivan (Purcell Basin, Mesoproterozoic)
Kochbulak (Kurama Belt, Altaides, Paleozoic)
Lega Dembi (Adola Greenstone Belt, Late Proterozoic)
Mt. Isa (Mt Isa Inlier, Mt Isa-McArthur Basin, Meso proterozoic)
Broken Hill, Curnamona Craton, Wylliama Supergroup, (Early-Middle Proterozoic)
epithermal
skarn
VHMS
SEDEX
orogenic Au

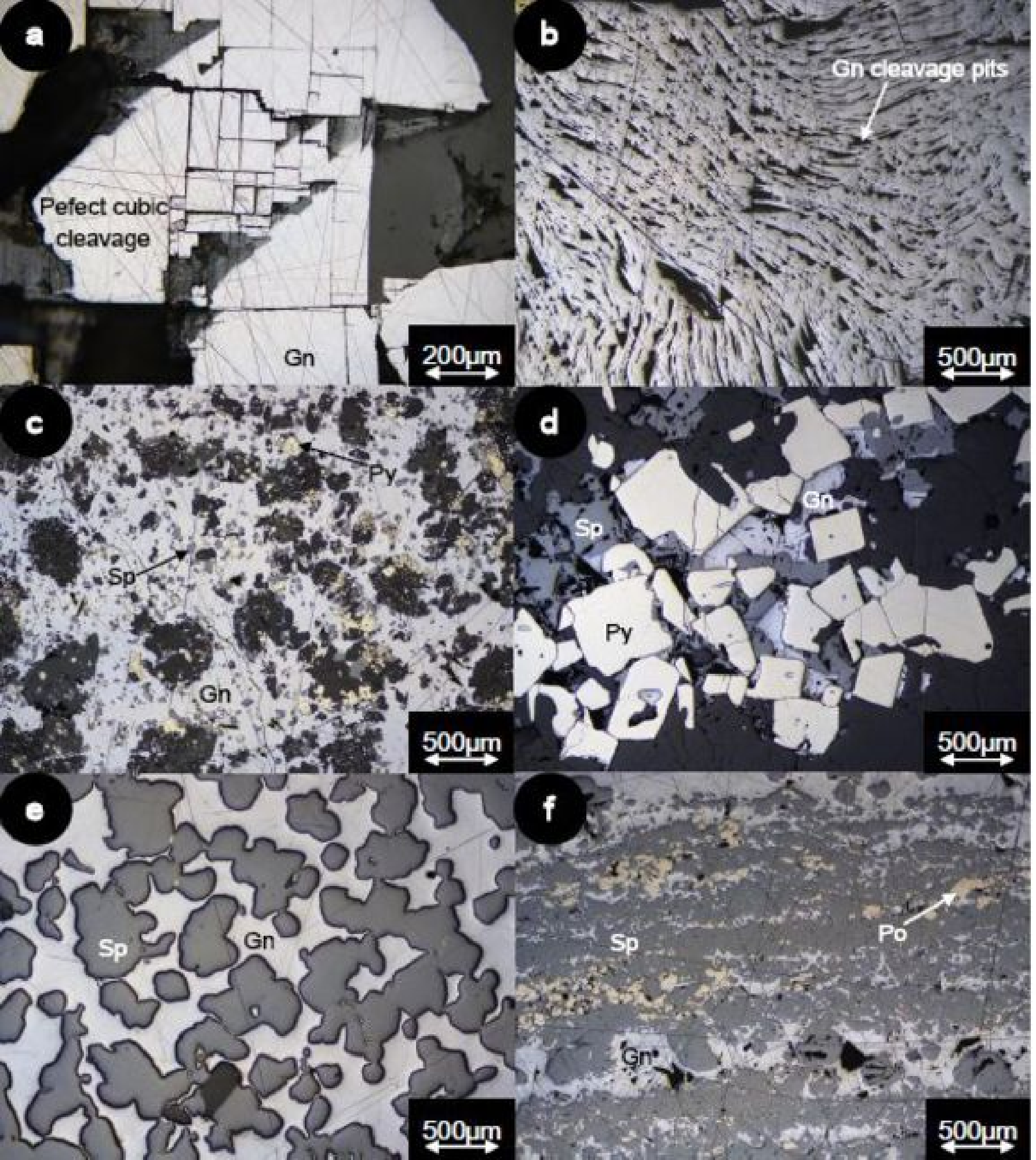
a
Pefect cubic cleavage
Gn
200µm
b
Gn cleavage pits
500µm
c
Py
Sp
Gn
500µm
d
Gn
Sp
Py
500µm
e
Sp
Gn
500µm
f
Po
Sp
Gn
500µm

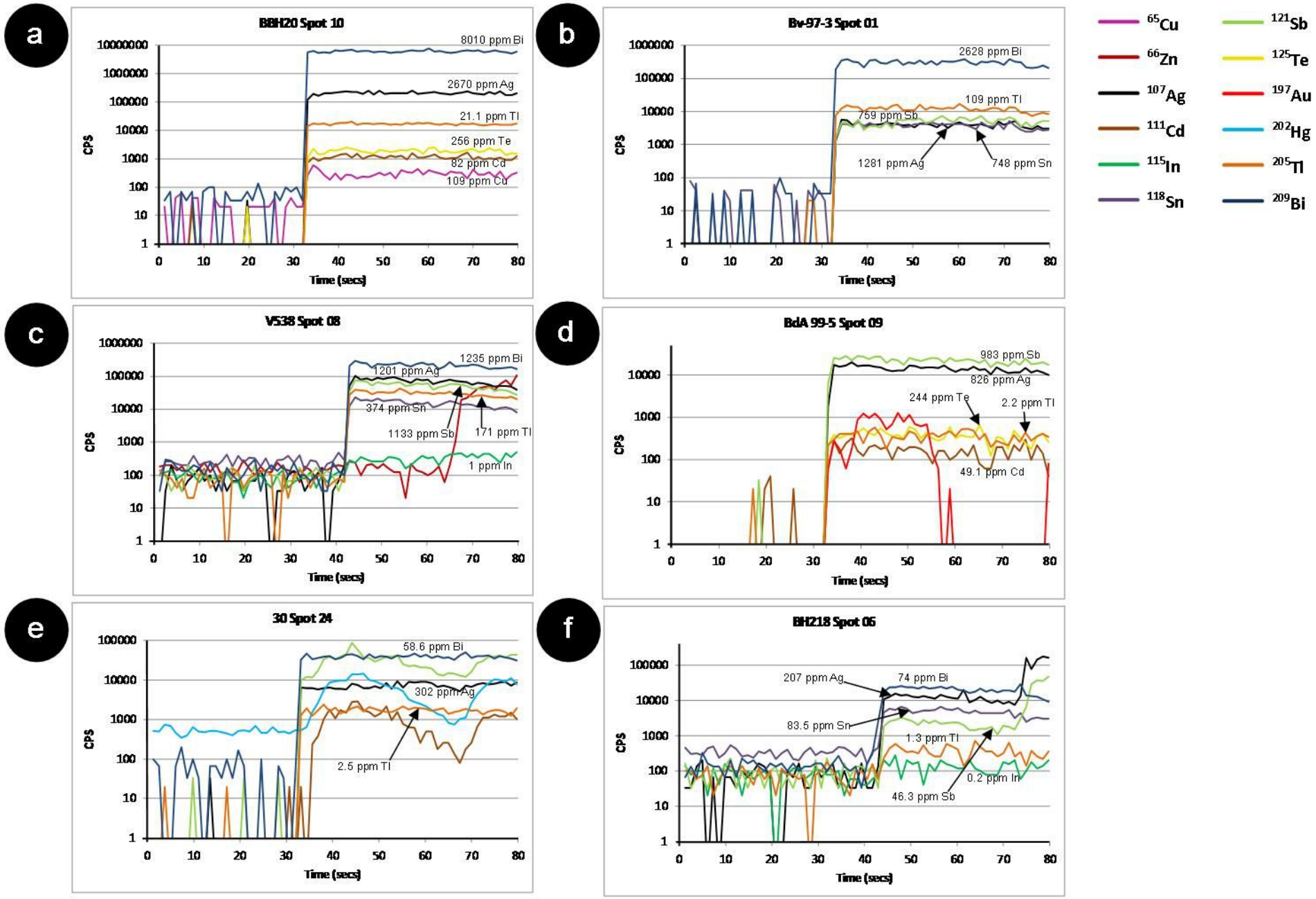
a
BBH20 Spot 10
8010 ppm Bi
2670 ppm Ag
21.1 ppm Tl
256 ppm Te
82 ppm Cd
109 ppm Cu
b
Bv-97-3 Spot 01
2628 ppm Bi
109 ppm Tl
759 ppm Sb
1281 ppm Ag
748 ppm Sn
c
V538 Spot 08
1235 ppm Bi
1201 ppm Ag
374 ppm Sn
1133 ppm Sb
171 ppm Tl
1 ppm In
d
BdA 99-5 Spot 09
983 ppm Sb
826 ppm Ag
244 ppm Te
2.2 ppm Tl
49.1 ppm Cd
e
30 Spot 24
58.6 ppm Bi
302 ppm Ag
2.5 ppm Tl
f
BH218 Spot 06
207 ppm Ag
74 ppm Bi
83.5 ppm Sn
1.3 ppm Tl
0.2 ppm In
46.3 ppm Sb
CPS
Time (secs)
65Cu
66Zn
107Ag
111Cd
115In
118Sn
121Sb
125Te
197Au
202Hg
205Tl
209Bi

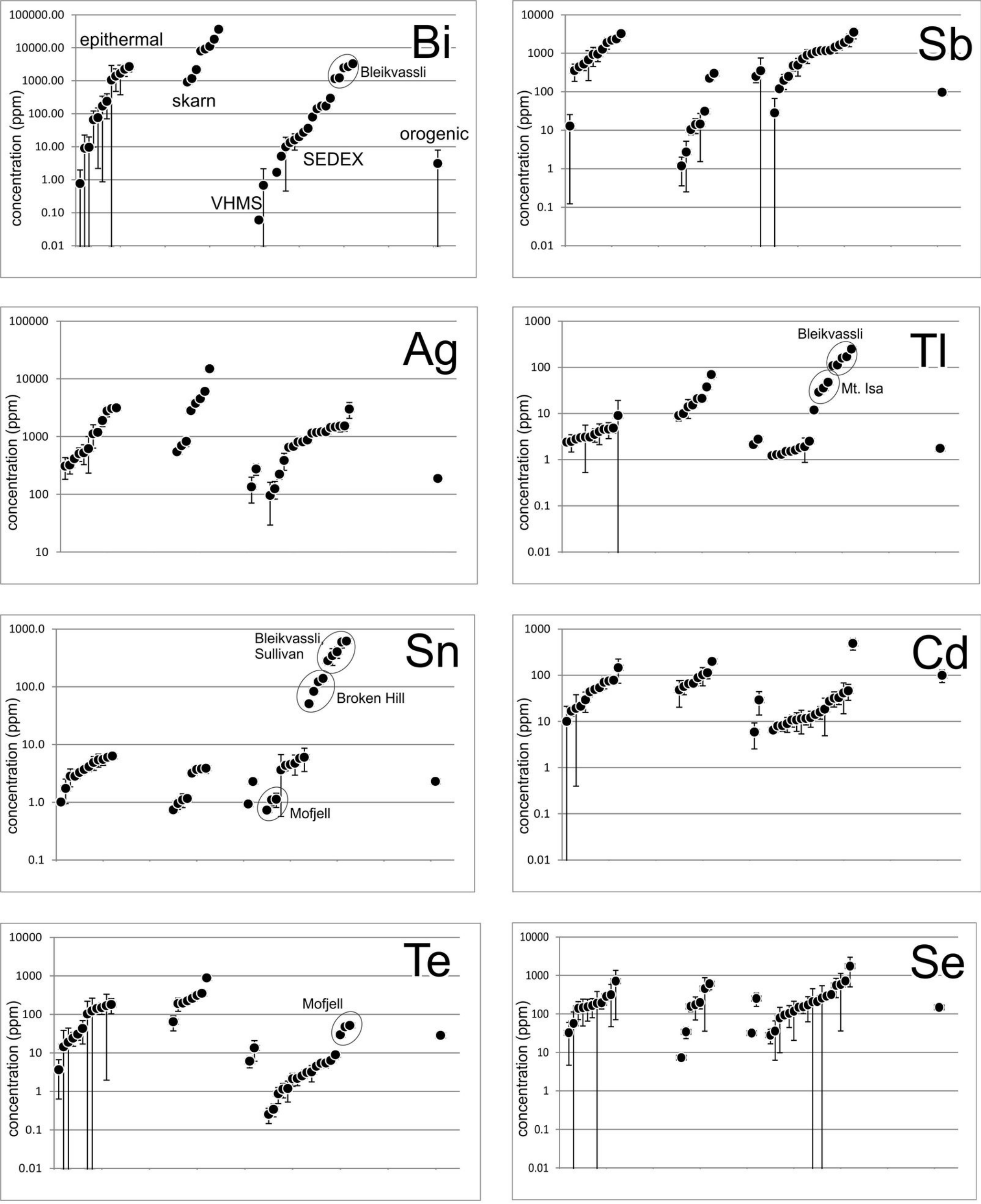

George et al. Figure 4

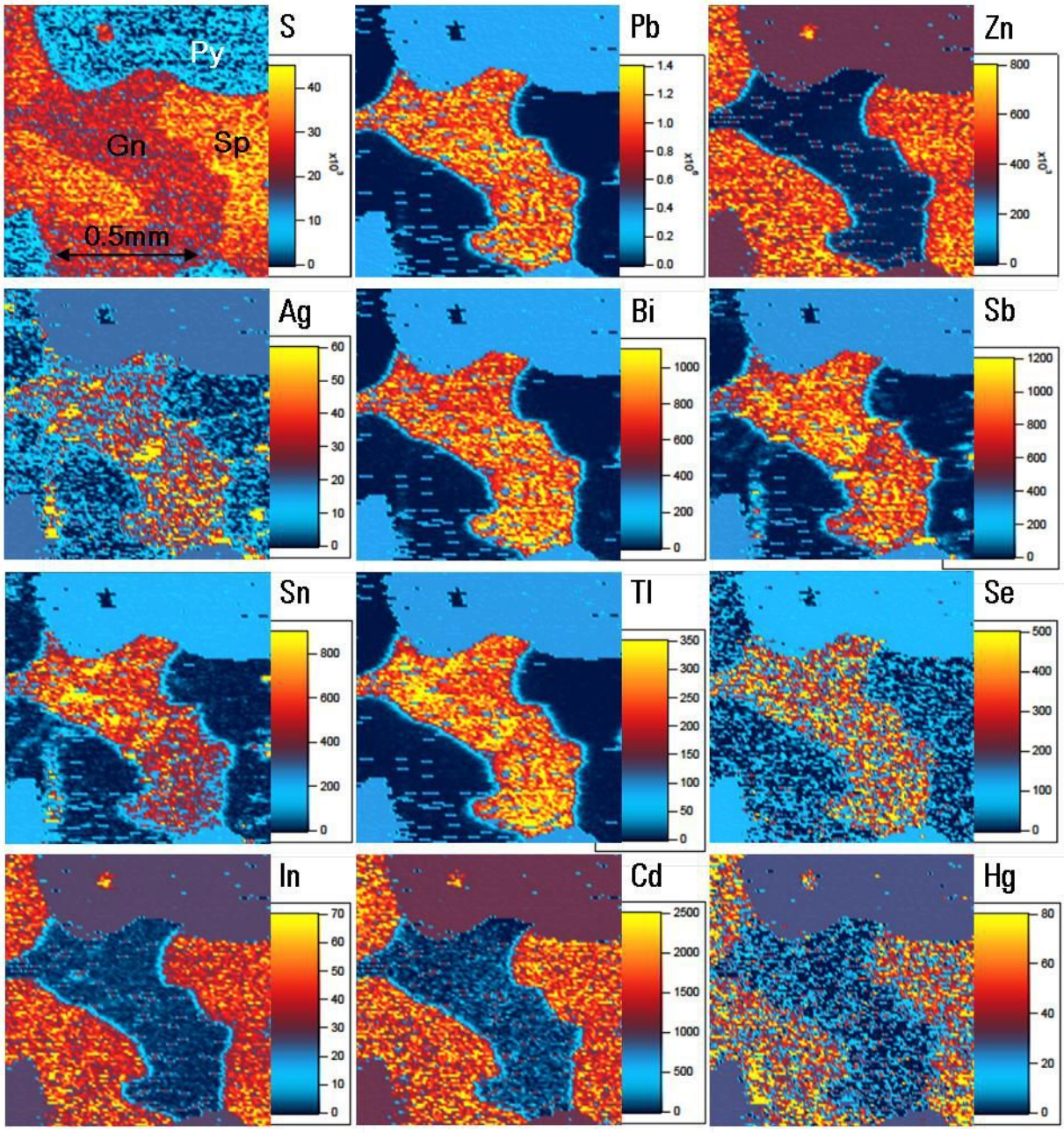
S
Py
Gn
Sp
0.5mm
Pb
Zn
Ag
Bi
Sb
Sn
Tl
Se
In
Cd
Hg

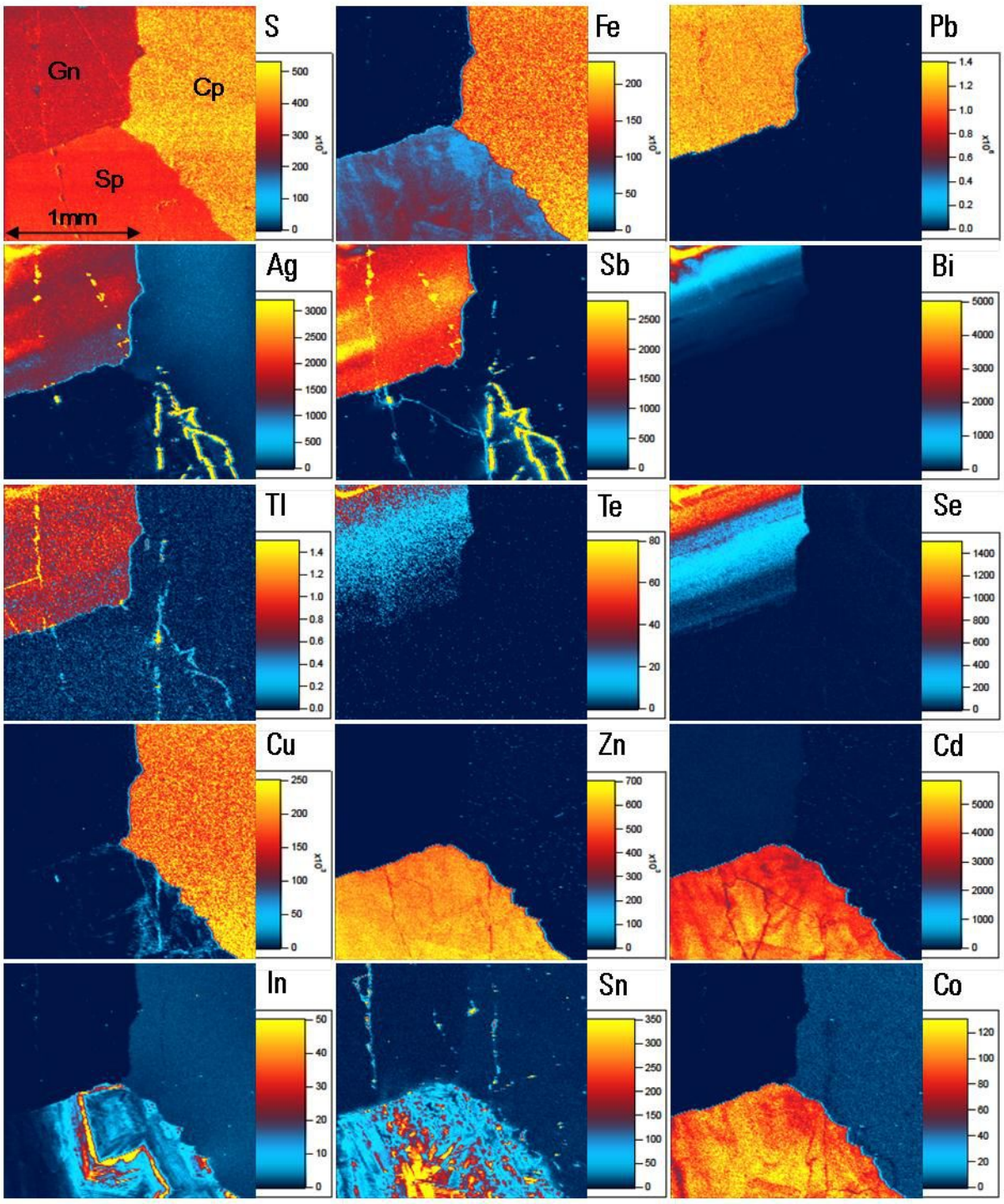
Gn
Cp
Sp
1mm
S
Fe
Pb
Ag
Sb
Bi
Tl
Te
Se
Cu
Zn
Cd
In
Sn
Co

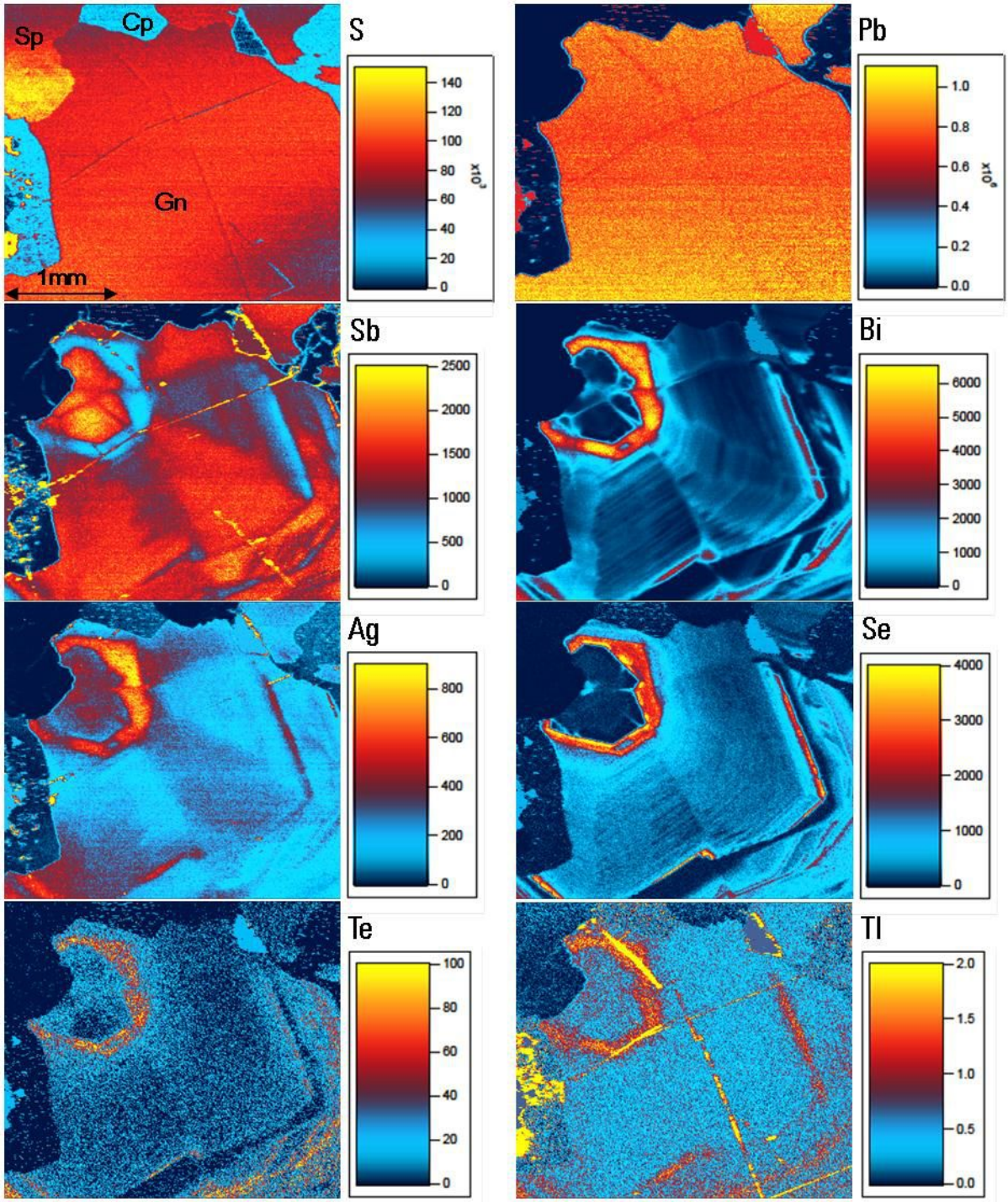
Sp
Cp
Gn
1mm
S
140
120
100
80
60
40
20
0
x10³
Pb
1.0
0.8
0.6
0.4
0.2
0.0
x10⁶
Sb
2500
2000
1500
1000
500
0
Bi
6000
5000
4000
3000
2000
1000
0
Ag
800
600
400
200
0
Se
4000
3000
2000
1000
0
Te
100
80
60
40
20
0
Tl
2.0
1.5
1.0
0.5
0.0

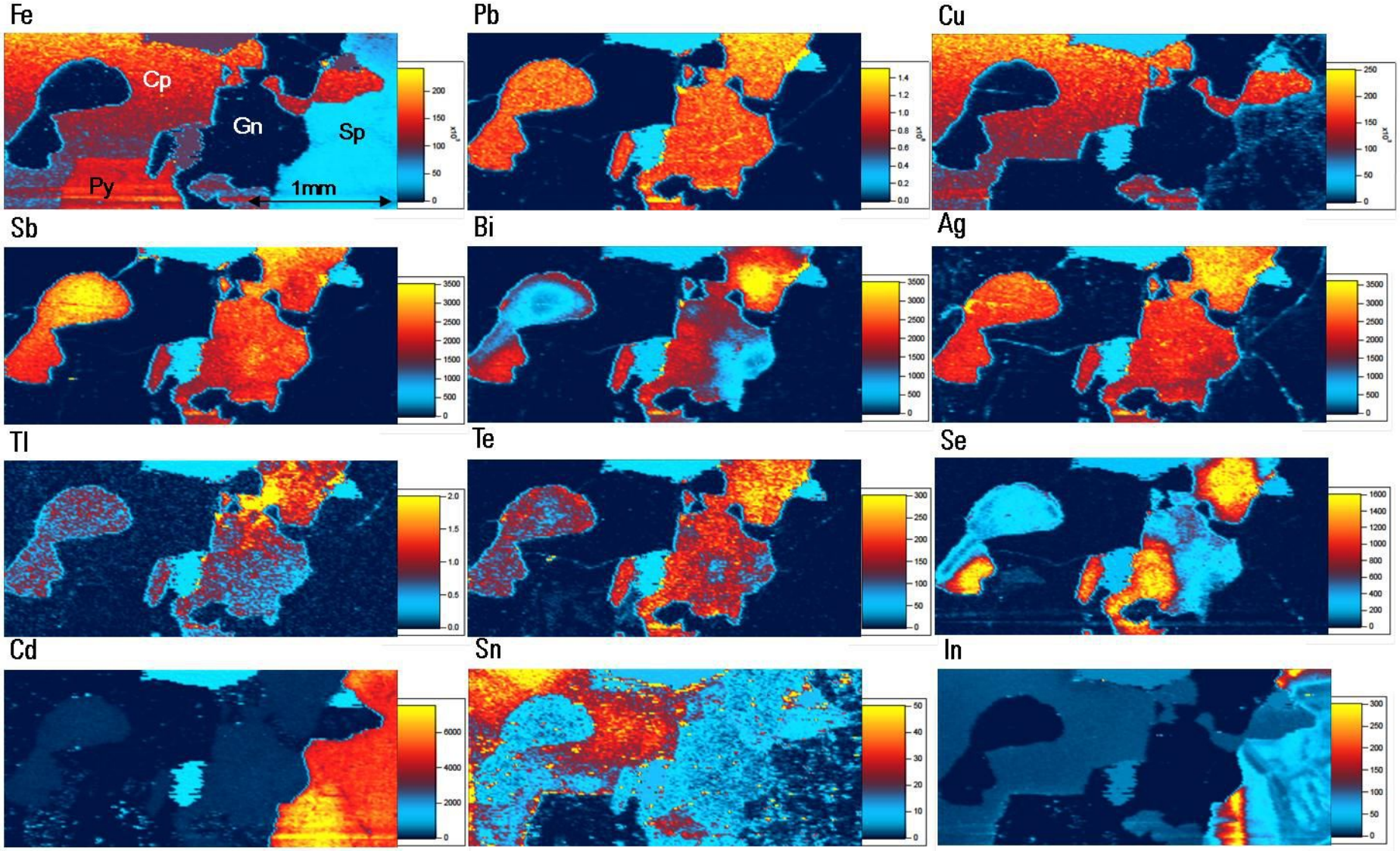
Fe
Cp
Gn
Sp
Py
1mm
Pb
Cu
Sb
Bi
Ag
Tl
Te
Se
Cd
Sn
In

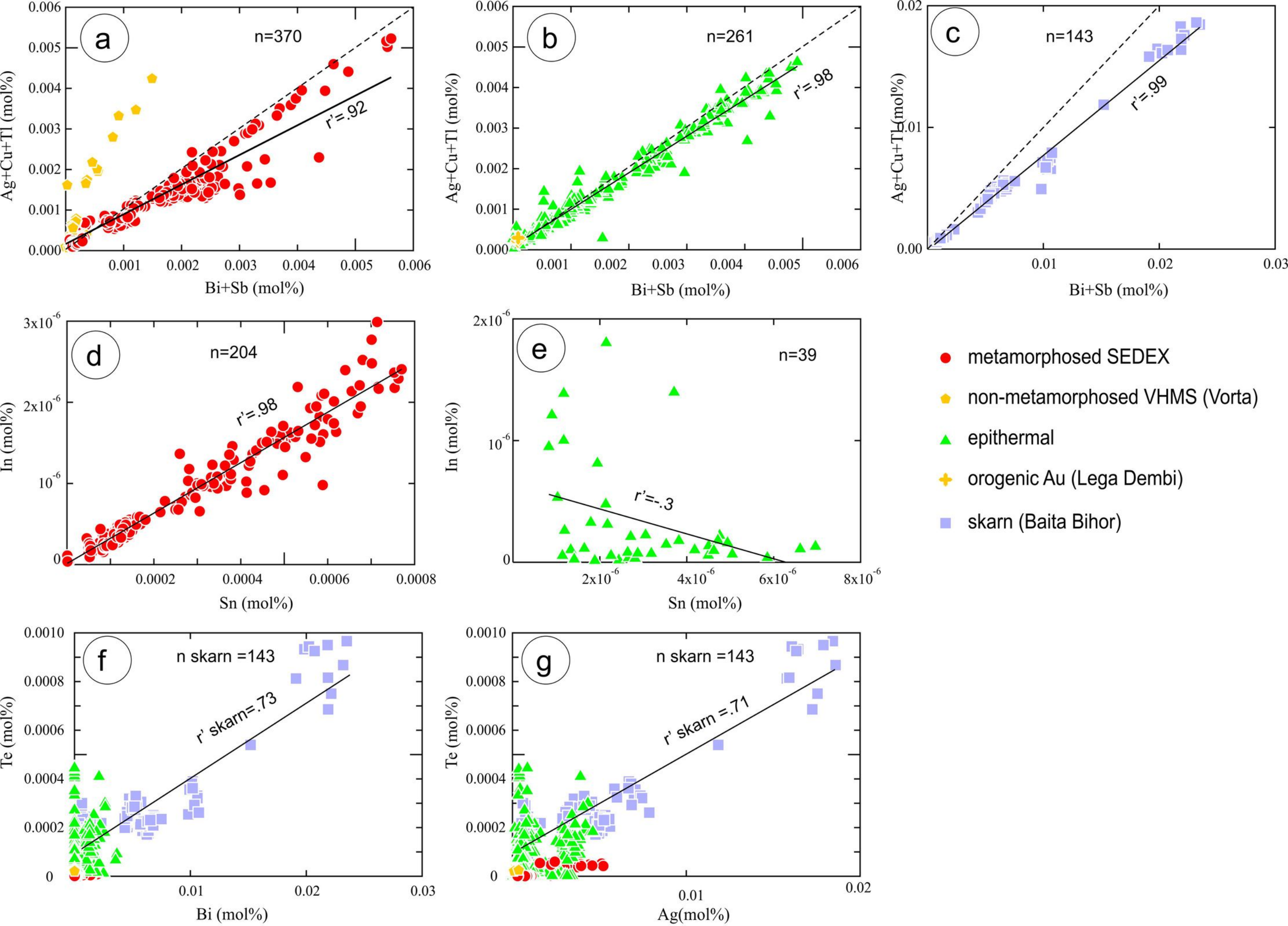

George et al. Figure 9